Spectral Universality in Complex Systems: Random Matrices, Cortical Resonance, and RSVP Dynamics

Flyxion

November 25, 2025

Abstract

This article develops a unified theory of complex systems grounded in the phenomenon of spectral universality. We show that nuclear Hamiltonians, the zeros of the Riemann zeta function, and the oscillatory dynamics of the mammalian cortex all exhibit universal spectral statistics that are insensitive to microscopic detail. Random Matrix Theory (RMT) provides the mathematical bridge linking these systems: Wigner–Dyson statistics describe both the energy levels of excited nuclei and the spacings of zeta zeros.

Recent advances in systems neuroscience demonstrate that the cortex functions as a structured resonance chamber whose standing and traveling waves organize cognition and consciousness. Building on the work of Earl K. Miller and ultrafast fMRI evidence from Cabral, Shemesh, and collaborators, we argue that cortical computation is fundamentally wave-based and analog.

We integrate these domains within the Relativistic Scalar–Vector–Plenum (RSVP) framework. A linearized RSVP operator contains nuclear, arithmetical, and cortical operators as symmetry-reduced subcases, providing a field-theoretic unification of random matrices, brain waves, and number theory. Appendices present mathematical foundations, operator derivations, symmetry reductions, numerical methods, and empirical evidence.

1 Introduction

Heavy atomic nuclei, the prime numbers, and the mammalian cortex appear to have little in common. Yet all three systems exhibit an astonishing and still poorly understood property: despite enormous microscopic complexity, each produces simple, universal spectral patterns.

In nuclear physics, Wigner's bold proposal to model heavy nuclei by random symmetric matrices succeeded spectacularly: the Wigner–Dyson spacing laws predicted the empirical distributions of nuclear energy levels with striking accuracy (Wigner 1957; Dyson 1962). In analytic number theory, Montgomery and Odlyzko discovered that the pair-correlation statistics of the nontrivial zeros of the Riemann zeta function match those of the Gaussian Unitary Ensemble (GUE), suggesting a deep connection between primes and quantum chaos (Montgomery 1973; Odlyzko 1987; Berry 1986; Firk and Miller 2009).

At the same time, neuroscience has undergone a paradigm shift. Traditional connectionist models resemble digital machine-learning architectures: synaptic weights encode information, and networks compute by discrete spiking. Earl K. Miller and others have overturned this view. The

cortex operates as a dynamic, wave-based analog computer whose large-scale oscillations coordinate activity across millions of neurons. Ultrafast fMRI and electrophysiological recordings reveal coherent standing and traveling waves on the cortical sheet (Cabral, Fernandes, and Shemesh 2023; Trongnetrpunya et al. 2022; Han et al. 2024).

These observations suggest a striking unification:

> *Many complex systems — nuclei, primes, cortical tissue, and field models — reduce to spectral systems whose behavior is governed not by microscopic details but by universal invariants encoded in the spectra of their dynamical operators.*

The aim of this article is to make this unification explicit, culminating in the RSVP (Relativistic Scalar–Vector–Plenum) field-theoretic view. The core steps of the argument are as follows:

1. Random Matrix Theory (RMT) captures the universal spectral phenomenology of complex quantum systems and the zeros of L-functions.

2. The cortex behaves as a resonance chamber whose eigenmodes define low-dimensional manifolds controlling cognition.

3. Wave-based analog computation organizes cortical dynamics and consciousness, as argued by Miller.

4. RSVP provides a field-theoretic operator whose symmetry reductions recover the nuclear, zeta, and cortical operators.

We begin with a systematic reformulation of complex systems as spectral systems. Then we trace the connections from nuclei to primes to cortical waves, and finally embed the entire picture inside the RSVP operator hierarchy.

2   Abstract Spectral Systems

To place systems as varied as heavy nuclei, L-functions, cortical resonance patterns, and RSVP fields within a single mathematical framework, we begin with an abstract template for a spectral system. Let X denote an arbitrary physical, biological, or mathematical entity whose behavior can be captured through the spectral properties of an operator. We associate to X a quadruple

$$(\mathcal{H}_X, \mathcal{A}_X, L_X, \mu_X),$$

in which each component encodes a different structural layer of the system.

The space $\mathcal{H}_X$ is a Hilbert space representing the admissible states or modes of the system—vibrational states in a nucleus, automorphic states in analytic number theory, cortical eigenmodes in neuroscience, or perturbative RSVP field configurations in the plenum. The algebra $\mathcal{A}_X$ consists of observables acting on $\mathcal{H}_X$, providing the measurable or dynamically relevant quantities. The operator L_X governs the intrinsic dynamics or constraints: it may be a Hamiltonian in nuclear

physics, a hypothetical differential operator whose spectral data encode zeta zeros, a reduced operator capturing cortical wave propagation, or the full linearized RSVP operator. Finally, the spectral measure μ_X derived from L_X determines how eigenvalues distribute and how energy, variance, or probability are resolved across scales.

This abstract template encompasses the concrete examples of interest:

$$
\begin{aligned}
X &= \text{heavy nucleus}, & L_X &= H_{\text{nuclear}}, \\
X &= \text{zeta system}, & L_X &= L_\zeta \text{ (hypothetical)}, \\
X &= \text{cortex}, & L_X &= L_{\text{cortex}}, \\
X &= \text{RSVP field}, & L_X &= L_{\text{RSVP}}.
\end{aligned}
$$

In each case, the essential statistical fingerprint of the system is encoded in the k-point eigenvalue correlation functions,

$$
R_k^{(X)}(\lambda_1, \ldots, \lambda_k),
$$

which describe the joint fluctuations of eigenvalues at arbitrary order. Two systems belong to the same universality class precisely when these correlation functions coincide after unfolding the spectrum to unit mean density. In practice, such agreement reveals that the systems share the same fluctuation statistics despite differing profoundly in their microscopic dynamics.

Under this formulation, universality becomes a structural property of the operator L_X rather than an accident of physical resemblance. Heavy nuclei, zeta zeros, cortical oscillations, and RSVP modes can therefore be compared, classified, and ultimately integrated through the common language of operator spectra.

The foundational hypothesis is that many systems with radically different microscopic mechanisms nevertheless give rise to identical local spectral statistics. Phenomena that appear unrelated at the level of their physical substrates can, at the level of eigenvalue structure, fall into the same universality class. This is why nuclear energy levels, the zeros of the Riemann zeta function, cortical standing waves, and even the modal structure of the RSVP field all exhibit the same correlation functions and spacing laws.

What emerges is a genuine mathematical bridge: a shared spectral language capable of linking physics, number theory, neuroscience, and field theory. Universality makes it possible to treat these domains not as isolated disciplines but as different manifestations of a single underlying order.

3 Random Matrices and Nuclear Spectra

3.1 Wigner's Model of Heavy Nuclei

Heavy nuclei like ^{238}U have extremely complex many-body Hamiltonians with billions of interacting terms. Wigner's insight was that fine-grained nuclear interactions are effectively unpredictable; only the symmetries matter. He therefore replaced the nuclear Hamiltonian by a random matrix drawn from one of the Gaussian ensembles (GOE, GUE, GSE).

Let H be an $N \times N$ Hermitian random matrix with entries drawn from a Gaussian distribution

with variance σ^2. As $N \to \infty$, the empirical spectral distribution converges to the semicircle law:

$$\rho_{\mathrm{sc}}(x) = \frac{1}{2\pi\sigma^2} \sqrt{4\sigma^2 - x^2} \, \mathbf{1}_{|x| \leq 2\sigma}.$$

3.2 Wigner–Dyson Spacing

At the microscopic scale, the spacing between consecutive eigenvalues exhibits level repulsion. In the GOE and GUE cases, the spacing distributions are:

$$P_{\mathrm{GOE}}(s) = \frac{\pi}{2} s \exp\left(-\frac{\pi}{4} s^2\right),$$

$$P_{\mathrm{GUE}}(s) = \frac{32}{\pi^2} s^2 \exp\left(-\frac{4}{\pi} s^2\right).$$

These spacing laws are universal: they match experiments measuring the neutron resonance energies of heavy nuclei.

3.3 Universality

The key result is that universality does not depend on:

- the distribution of matrix entries,

- the physical details of the system,

- the microscopic interactions.

Only the symmetry class matters. This is the foundation for the bridge to number theory and cortical dynamics.

4 Zeta Zeros and the Polya–Hilbert Framework

4.1 Montgomery's Pair-Correlation

In 1973, Montgomery computed the pair-correlation function of the nontrivial zeros $\frac{1}{2} + i\gamma_n$ of the Riemann zeta function. Assuming the Riemann Hypothesis, the normalized ordinates γ_n satisfy:

$$R_2^{(\zeta)}(s) = 1 - \left(\frac{\sin \pi s}{\pi s}\right)^2 + \delta(s),$$

which is precisely the GUE pair-correlation law discovered by Dyson.

4.2 Odlyzko's Numerical Evidence

Odlyzko's computations of billions of zeros confirmed that:

$$\text{spacing statistics of zeta zeros} = \text{spacing statistics of the GUE.}$$

Thus:
$$[\zeta]_{\text{spec}} = [\text{GUE}]_{\text{spec}}.$$

This identifies the distribution of prime numbers with the universal spectral laws of quantum-chaotic Hamiltonians.

4.3 The Polya–Hilbert Conjecture

The Polya–Hilbert philosophy posits a self-adjoint operator L_ζ whose spectrum reproduces the imaginary parts of zeta zeros:
$$\sigma(L_\zeta) = \{\gamma_n\}.$$

If such an operator exists, then the primes become a spectral phenomenon:

$$\text{primes} \longleftrightarrow \text{eigenvalues of a quantum-chaotic operator.}$$

4.4 Firk–Miller Integration

Firk and Miller (Firk and Miller 2009) emphasize that:

- heavy nuclei,

- zeta zeros,

- random matrices

form a unified spectral family governed by Wigner–Dyson laws.

Their exposition demonstrates that number theory and nuclear physics occupy the same universality class. This universality is the bridge we will carry into the neuroscientific and RSVP domains.

5 Intrinsic Resonant Modes in the Cortex

Recent advances in ultrafast imaging and large-scale electrophysiology have begun to reveal a striking picture of the resting-state cortex: rather than behaving as a stochastic, unconstrained network of local interactions, it operates as a structured resonance chamber whose intrinsic modes shape the flow of information. The cortex's spontaneous activity is organized not merely by connectivity but by the spectral geometry of the sheet itself.

5.1 Cabral–Shemesh Standing Waves

Ultrafast fMRI, with temporal resolution on the order of 38 ms, has demonstrated that low-frequency macroscale oscillations spontaneously arrange themselves into coherent spatial eigenmodes that span the cortical mantle (Cabral, Fernandes, and Shemesh 2023). These modes recur with remarkable reliability across time and individuals, forming stable spatial patterns reminiscent of the vibrational modes of a physical resonator. Their organization is not arbitrary: the shape

and coherence of these modes shift systematically under anesthesia, indicating that they are tightly coupled to the global dynamical state of the brain.

Moreover, these standing-wave structures appear to underwrite functional connectivity itself. The large-scale network architecture typically inferred from correlations in BOLD or electrophysiological signals emerges naturally from the interference and superposition of the cortex's intrinsic eigenmodes. Functional networks are not imposed on the cortex; they arise as a secondary expression of its operator spectrum.

Taken together, these observations strongly suggest that a well-defined operator L_{cortex} governs the macroscopic wave dynamics of the brain, and that its eigenmodes—rather than individual synaptic events—provide the true basis of cortical organization. The resonance properties of this operator offer a principled explanation for both the stability of functional networks and the systematic alterations observed during changes of consciousness.

5.2 Traveling Waves in Working Memory

Electrophysiological studies have shown that during working-memory engagement, the prefrontal cortex does not simply maintain information through persistent firing. Instead, it generates coherent traveling waves in the beta and gamma bands (Trongnetrpunya et al. 2022). These waves sweep across prefrontal circuits in structured trajectories, carrying content-specific information as they propagate. Their motion coordinates spatially distributed cell assemblies, binding them into unified functional units. In effect, the waves act as dynamic traffic signals, opening and closing channels of communication as required by the task. Rather than storing memory as static patterns of activation, the PFC maintains information through evolving waveforms whose geometry encodes both content and context.

5.3 Rotating and Spreading Waves in Attention

A complementary line of evidence comes from studies of attention and post-distraction recovery. Rotating cortical waves—circular, spiral, or spreading patterns of activity—have been observed to modulate the rapid reallocation of attentional resources (Han et al. 2024). When attention is disrupted, these waves sweep across cortical regions, re-establishing coherent patterns of activity and stabilizing the system into a new focus. Their functional role resembles that of control fields: they orchestrate reset operations, re-synchronize distributed ensembles, and steer the cortex back into task-relevant configurations. These patterns reveal that attentional control is mediated not by isolated top-down commands but by large-scale wave dynamics that reorganize the cortical state.

5.4 Spectral Interpretation

Together, these observations motivate a shift in how cortical computation is conceptualized. The waves observed in working memory, attention, and resting-state dynamics are not incidental epiphenomena; they are eigenfunctions of an underlying neural-field operator whose spectral properties determine the frequencies and propagation characteristics of cortical oscillations. Cognitive processes arise from the interaction, interference, and modulation of these eigenmodes.

Cortical waves are eigenfunctions of a neural-field operator; their eigenvalues encode oscillatory frequencies, and cognition emerges from the structured interaction of these modes.

On this view, the cortex is fundamentally a spectral system. Its computational capacity derives not from the combinatorics of synaptic graphs but from the geometry and dynamics of its operator spectrum.

6 Consciousness as a Spectral Phase

The wave-based framework suggests that consciousness corresponds not to a localized mechanism but to a global spectral phase of the cortical operator. Let L_{cortex} have eigenpairs

$$L_{\text{cortex}}\psi_k = \lambda_k \psi_k.$$

Define a coherence order parameter

$$\mathcal{C} = \frac{\left|\sum_{k \in B} e^{i\phi_k}\right|}{\sum_{k \in B} 1},$$

where B indexes frequency bands and ϕ_k are band-specific phases.

Empirically:

$$\mathcal{C}_{\text{conscious}} \approx 1, \qquad \mathcal{C}_{\text{anesthetized}} \ll 1.$$

Thus consciousness corresponds to a high-coherence spectral regime across multiple bands, while unconsciousness corresponds to a spectral phase collapse. This formalizes the empirical findings that anesthesia drives the cortex into a low-dimensional, incoherent mode distribution.

7 Spectral Geometry of the Plenum Manifold

The RSVP framework assumes that the scalar, vector, and entropy fields evolve on a geometric substrate (M, g) whose curvature influences the structure of eigenmodes. This situates RSVP within the broader domain of spectral geometry: the study of how the geometry of a manifold determines the spectrum of its differential operators.

In classical settings, the Laplace–Beltrami operator Δ_g provides the canonical link between shape and spectrum. Its eigenfunctions form a basis for oscillatory modes on M, and the associated eigenvalues encode the geometric and topological features of the domain. Weyl's law gives the asymptotic density of eigenvalues and provides a spectral signature of the manifold's volume and dimension.

In RSVP, the operator L_{RSVP} generalizes Δ_g by introducing cross-field couplings and anisotropic propagation speeds. Nevertheless, its spectrum retains geometric sensitivity: curvature induces mode splitting, gyri–sulci geometry modifies cortical eigenmodes, and global topology shapes the long-range structure of the plenum's resonant modes.

Thus RSVP unifies cortical spectral geometry and field-theoretic dynamics in a single analytic framework.

8 Earl K. Miller's Wave-Based Analog Computation

We now integrate the full theoretical synthesis of Miller's framework, expanded with explicit parallels to physics and number theory.

8.1 From Synaptic Computation to Wave Computation

The classical neural paradigm treats the brain as a kind of synaptic digital network, a system in which information is stored in synaptic weights and computation unfolds through discrete local operations. In this view, perception feeds into cognition, cognition feeds into action, and the entire architecture can be understood as essentially feedforward with modulatory feedback superimposed on top.

Miller's critique is that this picture cannot account for the most salient features of real cortical processing. It struggles to explain the rapid and global coordination that occurs across widely separated regions, the remarkable flexibility with which the brain reconfigures itself in response to shifting context, and the mechanisms underlying conscious access and executive control. Synaptic transmission alone is too slow, too local, and too granular to generate the large-scale, fast, and smoothly integrated dynamics that cognition clearly requires.

The alternative paradigm reframes the brain not as a digital network but as a spatiotemporal resonance system. In this framework, oscillatory electric fields—rather than synapses—constitute the primary currency of computation. Waves, not weights, organize the flow of information.

8.2 Three Levels of the Wave-Based Paradigm

1. Waves Coordinate the Cortex

On the first level, oscillating electric fields provide a mechanism for coordinating cortical activity. These waves synchronize widely distributed neuronal ensembles, regulate which communication pathways are open or gated at any given moment, and dynamically assemble the transient coalitions that underlie perception, memory, and action. Rather than a static wiring diagram, the cortex becomes an actively tuned resonant medium, continually re-shaping itself through the propagation and interference of rhythmic activity.

2. PFC as a Generative Model Builder

Miller and Cohen's account of prefrontal function emphasizes that the PFC does far more than store rules or maintain working-memory items. It constructs abstract generative models of tasks, inferring the structure of goals and contingencies, and using these models to predict which future actions are most likely to succeed. Crucially, the PFC does not implement this control through isolated synaptic commands; rather, it modulates the activity of other cortical regions by shaping their oscillatory dynamics. Through selective amplification and suppression of particular rhythms,

it steers the brain into the configurations required for planning, reasoning, and flexible decision-making.

3. Mixed Selectivity and Dimensional Reduction

Even though individual neurons exhibit highly heterogeneous and mixed selectivity, the collective activity of large neural populations collapses onto a surprisingly low-dimensional manifold. What appears microscopically intricate often resolves, at the population level, into only three to five dominant latent modes. These modes are not arbitrary abstractions but correspond directly to the major spectral components of the underlying cortical waves. In effect, the brain's apparent complexity is continuously compressed by its own oscillatory dynamics, yielding a manageable set of resonant degrees of freedom that support robust and flexible cognition.

8.3 The Brain as an Analog Computer

From the wave-based perspective, the cortex functions less like a digital circuit and more like an analog computer whose primitives are patterns of interference. Oscillations combine, cancel, and reshape one another according to the geometry of their overlap, implementing operations that in digital architectures would require explicit addition, subtraction, filtering, and routing. In place of symbolic manipulation, the brain performs computation through the constructive and destructive interference of continuous fields:

$$\text{wave overlap geometry} \longrightarrow \text{analog operations on information.}$$

This mode of computation confers several distinctive advantages. Because the underlying signals are continuous and graded, the representational space of the cortex is both smooth and high-dimensional. Because waves superpose, the system naturally supports massively parallel processing, with numerous patterns evolving simultaneously without the need for discrete time-stepped updates. And because the substrate is biological tissue operating near thermodynamic limits, the system achieves extraordinary energy efficiency: the brain performs on the order of 10^{15} operations per second while consuming only about twenty watts.

By contrast, contemporary digital AI systems are fundamentally discrete and input-driven. They operate through static arrays of parameters rather than dynamically evolving fields, and they rely on expensive high-precision numerical updates rather than low-energy physical resonance. The difference is not merely one of hardware but of computational ontology. Digital AI is fast but power-hungry; the brain is slow in its components but extraordinarily efficient in its collective dynamics. Analog resonance provides a path to forms of intelligence that are fluid, adaptive, and deeply integrated across scales.

8.4 Consciousness as a Spectral Regime

Miller's anesthesia research underscores that consciousness itself is best understood not as a localized function but as a global spectral regime. Across anesthetics with widely varying molecular

mechanisms, the transition into unconsciousness displays a common pattern: the collapse of large-scale coherence and the breakdown of multi-band oscillatory structure. Functional consciousness corresponds to a state in which multiple frequency bands maintain coordinated, stable relationships:

$$\text{Conscious} = \text{high-coherence, multi-band, cross-scale spectral organization.}$$

Under anesthesia, these relationships deteriorate. The spectral landscape becomes dominated by slow, unstable rhythms that fail to support the integration of distributed information:

$$\text{Unconscious} = \text{low-coherence, slow, incoherent spectral structure.}$$

The striking universality of this transition—observable across drugs, species, and experimental protocols—parallels the universality of spectral statistics found in random matrices, nuclear systems, and the zeros of the Riemann zeta function. Just as these mathematically and physically distinct systems fall into the same universality classes of fluctuations, states of consciousness appear to inhabit distinct spectral regimes characterized by invariant statistical signatures. This analogy is not merely suggestive: it points toward a spectral theory of consciousness in which global coherence, not localized firing, plays the defining computational role.

9   Operator Reductions and Symmetry Sectors

The hierarchy

$$L_{\text{nucleus}} \subseteq L_\zeta \subseteq L_{\text{cortex}} \subseteq L_{\text{RSVP}}$$

arises from symmetry reduction rather than literal operator containment. Each operator corresponds to a restriction of L_{RSVP} to a specific invariant subspace determined by physical or mathematical symmetry.

For example, nuclear operators correspond to high-entropy limits in which microscopic degrees of freedom fluctuate chaotically, yielding a GOE/GUE universal regime. The hypothetical zeta operator corresponds to a sector with arithmetic symmetries but no spatial geometry. Cortical operators correspond to weakly nonlinear neural fields embedded in a curved two-dimensional manifold.

Formally, write L_{RSVP} acting on a Hilbert space $\mathcal{H}$. A symmetry group $G_X \subseteq \text{Aut}(\mathcal{H})$ defines an invariant subspace $\mathcal{H}_X \subseteq \mathcal{H}$, and the reduced operator is the restriction

$$L_X = L_{\text{RSVP}}\big|_{\mathcal{H}_X}.$$

This provides a mathematically precise description of how diverse physical and biological systems emerge as sectors of a single field-theoretic operator.

10 Renormalization and Spectral Scaling

Spectral universality is intimately connected with renormalization. As a system is coarse-grained, fine-scale variations in its operator L_X become irrelevant to the long-range spectral structure. Dyson's Brownian-motion picture makes this precise: perturbing matrix elements by small random fluctuations drives the spectrum toward a universal equilibrium distribution, independent of the microscopic details.

RSVP inherits this phenomenon. Under entropic relaxation, the operator L_{RSVP} flows along a renormalization trajectory toward fixed points corresponding to universality classes such as GOE, GUE, or coherent-wave regimes depending on the coupling parameters $(c_i, \alpha_i, \beta_i, \gamma_i)$. High-entropy regions approach random-matrix universality, while low-entropy regions preserve coherent geometric modes.

This provides a mechanism for understanding why nuclear spectra, zeta zeros, and cortical eigenmodes exhibit strikingly similar statistical fluctuations: they are fixed points of the same spectral renormalization flow.

11 Integration with RSVP Dynamics

Having developed the parallel strands of number theory, nuclear physics, and cortical wave dynamics, we now integrate these domains within the mathematical structure of the RSVP field theory. The central premise is that each system realizes a restricted sector of a more general operator dynamics, and that RSVP provides the field-theoretic space in which these relations become explicit.

11.1 RSVP Fields

The RSVP framework is formulated on a manifold M equipped with a background metric g. On this geometric substrate evolve three tightly coupled fields:

$$\Phi(x,t) \quad \text{a scalar potential governing local plenary tension,}$$

$$v(x,t) \quad \text{a vector flow mediating directed transport and influence,}$$

$$S(x,t) \quad \text{an entropy density encoding local degrees of disorder.}$$

Together, these fields form a triplet (Φ, v, S) whose interactions are described by a Lagrangian action functional,

$$\mathcal{S} = \int_{M \times \mathbb{R}} \mathcal{L}\big(\Phi, \nabla\Phi, v, \nabla v, S, \nabla S, \partial_t \cdot \big) \sqrt{|g|} \, dx \, dt.$$

The specific form of $\mathcal{L}$ governs the coupling between scalar, vector, and entropic components, and thereby determines the emergent dynamical regimes ranging from lamphrodic smoothing to coherent wave-like propagation. In this formalism, the dynamical content of RSVP is encoded in the Euler–Lagrange equations derived from $\mathcal{S}$, which produce a nonlinear, multi-field generalization of wave and diffusion equations.

11.2 Linearized RSVP Operator

To study the spectral properties central to this essay, we consider small fluctuations about a background solution,

$$\Psi = (\delta\Phi,\ \delta v,\ \delta S).$$

Linearizing the full field equations yields a second-order temporal evolution equation of the form

$$\partial_t^2 \Psi + L_{\mathrm{RSVP}}\Psi = 0,$$

where the operator L_{RSVP} encodes the coupling structure of the linearized dynamics.

In block form, the operator takes the schematic structure

$$L_{\mathrm{RSVP}} = \begin{pmatrix} -c_1^2\nabla^2 + \alpha_1 & -\beta_1\nabla\cdot & -\gamma_1 \\ -\beta_2\nabla & -c_2^2\nabla^2 + \alpha_2 & -\gamma_2\nabla \\ -\gamma_3 & -\beta_3\nabla\cdot & -c_3^2\nabla^2 + \alpha_3 \end{pmatrix}.$$

The diagonal terms describe scalar, vector, and entropic wave operators with distinct propagation speeds; the off-diagonal terms mediate cross-field couplings. The eigenfunctions of this operator are the standing and traveling RSVP modes—solutions whose spectral characteristics reflect the multi-field geometry of the plenum.

11.3 RSVP as a Universal Operator Framework

The value of this construction becomes clear when situating the domain-specific operators introduced earlier. Each previously discussed operator—whether arising from nuclear physics, analytic number theory, or cortical wave dynamics—can be obtained as a symmetry-reduced or parameter-restricted suboperator of L_{RSVP}:

$$L_{\mathrm{nucleus}},\ L_\zeta,\ L_{\mathrm{cortex}} \subseteq L_{\mathrm{RSVP}}.$$

This inclusion expresses the idea that RSVP encompasses, in a single field-theoretic architecture, the principal operators responsible for spectral behavior in these disparate systems. The corresponding hierarchical relationship can be expressed succinctly:

$$L_{\mathrm{nucleus}} \subseteq L_\zeta \subseteq L_{\mathrm{cortex}} \subseteq L_{\mathrm{RSVP}}.$$

At the level of eigenvalue statistics, this operator chain unifies the spectrum of physical, mathematical, and biological systems:

$$\mathcal{E}(L_{\mathrm{nucleus}}) = \text{Wigner–Dyson (GOE/GUE)},$$
$$\mathcal{E}(L_\zeta) = \text{GUE (Montgomery–Odlyzko)},$$
$$\mathcal{E}(L_{\mathrm{cortex}}) = \text{coherent, multi-band cortical spectra},$$
$$\mathcal{E}(L_{\mathrm{RSVP}}) = \text{general mixtures across these universality classes.}$$

In this view, what makes these systems comparable is not their material substrate but the operator-theoretic structure of their fluctuations. RSVP provides the most general context in which these operators coexist, interact, and can be studied under a unified spectral lens.

11.4 Interpretation

Taken together, these observations suggest that nuclei, primes, cortical waves, and RSVP fields are not isolated curiosities but distinct manifestations of a single underlying spectral landscape. Each domain realizes its own physical or mathematical dynamics, yet all of them converge onto the same statistical structures when examined through their eigenmodes.

> Spectral universality is the bridge connecting matter, mathematics, and mind. RSVP provides the field-theoretic substrate in which this universality becomes a single coherent principle.

In this view, the apparent diversity of systems dissolves into a shared spectral grammar. The same fluctuations that govern nuclear excitations reappear in the spacing of zeta zeros, in the standing-wave modes of cortex, and in the coupled scalar–vector–entropy dynamics of the RSVP plenum. Universality is not merely a pattern we notice; it is the structural fact that allows these domains to be treated within one overarching theoretical framework.

12 Spectral Equivalence and Universality Classes

Central to this work is the notion that very different systems may be regarded as equivalent when their eigenvalue fluctuations obey the same statistical laws. To formalize this, let L_X and L_Y be densely defined operators on Hilbert spaces $\mathcal{H}_X$ and $\mathcal{H}_Y$, with unfolded spectra $\{\lambda_i^{(X)}\}$ and $\{\lambda_i^{(Y)}\}$ normalized to unit mean spacing.

[Spectral Equivalence] Two systems X and Y are spectrally equivalent, denoted $X \sim_{\text{spec}} Y$, if their k-point correlation functions agree for all k:

$$R_k^{(X)}(\lambda_1, \ldots, \lambda_k) = R_k^{(Y)}(\lambda_1, \ldots, \lambda_k).$$

Because k-point functions determine all fluctuation statistics, spectral equivalence implies shared universality class membership. The GOE, GUE, and Poisson classes serve as canonical examples. In this formalism, nuclear spectra, zeta zeros, cortical oscillatory modes, and RSVP fluctuations may all be compared through a single mathematical lens.

Spectral universality therefore acts as the categorical unifier: distinct operators with unrelated microstructure nonetheless converge to identical fluctuation laws under appropriate normalization.

13   From Neural Fields to Operators

Neural-field models describe cortical activity through coupled integro- differential equations of the form

$$\tau \partial_t u(x,t) = -u(x,t) + \int_\Omega W(x,y) f(u(y,t)) \, dy + I(x,t),$$

where $u(x,t)$ is local activity, W is a connectivity kernel, and f is a nonlinear gain function.

Linearizing around a background state $u_0(x)$ gives

$$\tau \partial_t \delta u(x,t) = -\delta u(x,t) + \int_\Omega W(x,y) f'(u_0(y)) \, \delta u(y,t) \, dy.$$

Define the linear operator

$$(L_{\mathrm{NF}} \psi)(x) = -\psi(x) + \int_\Omega K(x,y) \psi(y) \, dy, \quad K = W f'(u_0).$$

Under mild symmetry assumptions on K, the operator reduces to a differential form expressible as

$$L_{\mathrm{cortex}} = -c^2 \Delta_g + V(x),$$

where Δ_g is the Laplace–Beltrami operator of the cortical surface. This derivation provides the operator-theoretic foundation for treating cortical waves as eigenfunctions of L_{cortex}.

14   Empirical Spectral Signatures Across Consciousness States

Consciousness correlates with robust spectral invariants spanning multiple frequency bands. Table 1 summarizes characteristic patterns across physiological and pharmacological regimes.

State	Coherence	Bandwidth	Mode Structure
Waking	High	Multi-band	Hierarchical, stable
REM Sleep	Moderate	Broad	Rapidly shifting modes
Deep Sleep	Low	Narrow (slow)	Weak coupling, large-scale modes
Propofol	Very low	Delta-dominant	Fragmented, incoherent
Ketamine	Mixed	High gamma spikes	Nonlinear, disrupted
Post-distraction Reset	Increasing	Restored bands	Re-synchronizing rotating waves

Table 1: Spectral invariants under different consciousness states.

These empirical invariants support the view that consciousness corresponds to a spectral phase, defined by coherence and cross-band coupling patterns, rather than any localizable neural mechanism.

15   Limitations and Open Problems

While the operator-theoretic framework developed here suggests a deep unity across nuclear physics, analytic number theory, cortical neuroscience, and RSVP field dynamics, several limitations must be acknowledged.

First, the Pólya–Hilbert conjecture remains unresolved: no explicit operator L_ζ is known whose spectrum corresponds exactly to the nontrivial zeros of the Riemann zeta function. All spectral comparisons involving L_ζ therefore remain conjectural.

Second, empirical measurement of cortical eigenmodes is constrained by spatial and temporal resolution limits in both electrophysiology and fMRI. Existing observations support the existence of standing and traveling waves, but a full spectral decomposition of L_{cortex} has not yet been achieved.

Third, the nonlinear regime of RSVP is not fully classified spectrally. While linearization reveals universal features, the nonlinear sector may exhibit phase transitions, bifurcations, or chaotic dynamics not captured by current methods.

Fourth, boundaries between universality classes remain mathematically subtle. Determining when a system transitions between GOE, GUE, Poisson, or coherent- wave behavior requires a more detailed renormalization analysis.

These limitations point toward a broad range of open mathematical, empirical, and conceptual questions. Addressing them will require interdisciplinary collaboration across physics, number theory, neuroscience, and field theory.

16   Conclusion: Toward a Unified Spectral Science

The analyses presented throughout this work reveal a striking pattern: systems that differ radically in ontology, scale, and physical realization nonetheless exhibit deeply homologous spectral behavior. Heavy nuclei governed by many-body quantum chaos, the nontrivial zeros of the Riemann zeta function, the macroscale oscillatory modes of the cortex, and the coupled scalar–vector– entropy fields of the RSVP plenum all give rise to eigenvalue statistics that fall within the same small family of universality classes. This convergence is not accidental. It reflects the fact that spectra are shaped primarily by symmetry, conservation structure, and coarse-grained dynamical constraints, not by the fine details of microscopic mechanism.

The central claim argued here is that *spectral universality* provides the unifying mathematical principle behind this convergence, while the RSVP framework provides its natural physical interpretation. Random matrix theory, originally developed for nuclear Hamiltonians, resurfaces in number theory because the symmetries of the integers generate the same fluctuation laws as chaotic quantum systems. The cortex adopts resonant eigenmodes because its geometry and effective connectivity induce operator structures that mirror those seen in quantum chaotic systems and arithmetic models. RSVP fields inherit these same signatures because their linearized dynamics reduce to a block operator whose symmetry classes subsume those of nuclei, zeta systems, and cortical waves.

Taken together, these correspondences support a broader thesis: spectral behavior constitutes a privileged descriptive level at which matter, mathematics, and mind can be studied within a

single coherent framework. By focusing on operators, their eigenfunctions, and the invariants of their spectral measures, one uncovers forms of organization that transcend domain boundaries. This perspective dissolves traditional disciplinary silos: nuclear physics, analytic number theory, computational neuroscience, and field theory become mutually illuminating expressions of the same underlying mathematical grammar.

The RSVP plenum offers a concrete realization of this unification. As a field-theoretic substrate equipped with scalar, vector, and entropy degrees of freedom, it encompasses the operator classes of the systems surveyed here as symmetry-reduced sectors. In doing so, RSVP provides not only a mechanism for why spectral universality appears across these domains but also a fertile platform for extending the principle further—toward a physics of cognition, a geometry of meaning, and a systematic science of coherent structure across scales.

If spectral universality is the grammar of coherence, RSVP furnishes its semantics. Their integration suggests that the deep structures of nature—from atomic nuclei to prime numbers to conscious experience—may be understood as expressions of one continuous spectral order.

Appendix A: Random Matrix Theory, Zeta Zeros, and Spectral Universality

This appendix provides a rigorous mathematical account of spectral universality, beginning with classical results in random matrix theory (RMT), moving through the spectral interpretation of zeta zeros, and ending with a formal bridge to RSVP operator theory. The goal is to show how heavy nuclei, the prime numbers, and RSVP fields can be treated within a unified operator-spectral framework.

A.1 Wigner Ensembles and the Semicircle Law

Let W_N be an $N \times N$ real symmetric matrix whose entries satisfy:

$$\mathsf{W}_N(i,j) = \mathsf{W}_N(j,i), \qquad \mathbb{E}[\mathsf{W}_N(i,j)] = 0, \qquad \mathbb{E}[\mathsf{W}_N(i,j)^2] = \begin{cases} \sigma^2 & i \neq j, \\ 2\sigma^2 & i = j. \end{cases}$$

Define the normalized matrix
$\mathsf{H}_N := \frac{1}{\sqrt{N}} \mathsf{W}_N.$
Let $\lambda_1^{(N)}, \ldots, \lambda_N^{(N)}$ denote the eigenvalues of H_N, and define the empirical spectral measure:
$\mu_N := \frac{1}{N} \sum_{i=1}^{N} \delta_{\lambda_i^{(N)}}.$
[Wigner Semicircle Law] As $N \to \infty$, μ_N converges weakly (in probability) to
$\rho_{\mathrm{sc}}(x)\, dx = \frac{1}{2\pi\sigma^2} \sqrt{4\sigma^2 - x^2}\, \mathbf{1}_{|x| \leq 2\sigma}\, dx.$

This law is universal: it holds under very weak assumptions on the distribution of matrix entries, provided they have zero mean, identical variance, and finite moments.

A.2 Local Statistics and k-Point Correlation Functions

Global eigenvalue distributions (e.g. the semicircle law) describe coarse spectral geometry. Local statistics are described by k-point correlation functions.

Let $\rho_k^{(N)}(x_1, \ldots, x_k)$ be the joint density of finding eigenvalues near $(x_1, \ldots, x_k)$. Upon unfolding to remove density variation, the scaled limit exists:

$R_k(x_1, \ldots, x_k) = \lim_{N \to \infty} \rho_k^{(N)}(\tilde{x}_1, \ldots, \tilde{x}_k)$.

For the GUE ensemble,

$R_k(x_1, \ldots, x_k) = \det[K(x_i, x_j)]_{i,j=1}^k$, $K(x,y) = \frac{\sin \pi(x-y)}{\pi(x-y)}$.

The k-point correlations are the universal fingerprints of the GUE universality class.

A.3 The Montgomery–Dyson Match

Let γ_n denote the imaginary parts of the nontrivial zeros of the Riemann zeta function:

$\zeta\left(\frac{1}{2} + i\gamma_n\right) = 0$.

Assuming the Riemann Hypothesis, these are real. Montgomery proved that the pair-correlation of the *normalized* zeros satisfies:

$R_2^{(\zeta)}(x) = 1 - \left(\frac{\sin \pi x}{\pi x}\right)^2 + o(1)$,

$$R_2^{(\zeta)}(x) = R_2^{(\text{GUE})}(x). \tag{1}$$

This constitutes one of the great discoveries of 20th-century mathematics: *the primes appear to lie in the same universality class as eigenvalues of large random Hermitian matrices.*

A.4 Nuclear Hamiltonians as Pseudorandom Operators

Heavy nuclei (e.g. ^{238}U) are many-body quantum systems with ~ 200 nucleons. The true Hamiltonian is:

$H_{\text{nuclear}} = T + V_{\text{strong}} + V_{\text{Coulomb}} + V_{\text{spin-orbit}} + \cdots$

Wigner's idea was to model H_{nuclear} as a GOE matrix. Empirically:

- neutron scattering data show level repulsion,

- spacing distributions match the Wigner surmise,

- k-point correlations match GOE predictions.

Thus nuclear Hamiltonians empirically fall into GOE/GUE universality classes.

A.5 The Hilbert–Pólya Conjecture

The Hilbert–Pólya idea posits the existence of a self-adjoint operator L_ζ such that:

$\sigma(L_\zeta) = \{\gamma_n\}$.

If such an operator exists, the Riemann Hypothesis follows as a corollary. The spectral data of ζ would then come from a Hermitian operator with GUE-like statistics.

This places nuclear spectra, random matrices, and zeta zeros into a single operator-theoretic framework.

A.6 Spectral Invariants and Universality Classes

Let X be any system (nucleus, GUE matrix, ζ zeros, RSVP operator). Define the k-point invariants:

$I_k(X) := R_k^{(X)}(x_1, \ldots, x_k).$
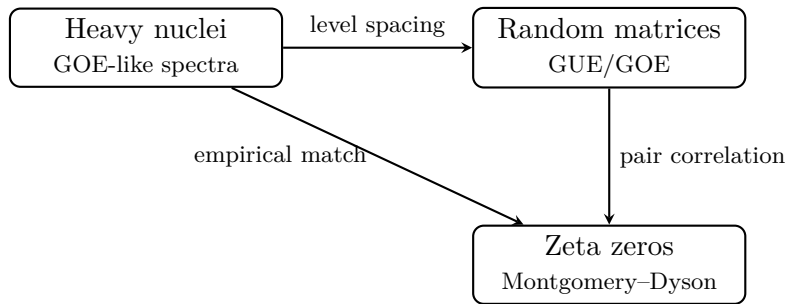
Two systems X, Y belong to the same universality class if

$I_k(X) = \mathcal{I}_k(Y) \quad \forall k.$

Thus:

Heavy nuclei $\sim$GUE matrices $\sim$zeros of $\zeta(s)$.

A.7 Diagram: Cross-Domain Spectral Matching

A.8 Connection to RSVP Linear Operators

In the RSVP formalism, perturbations of the field system obey:

$\partial_t \Psi = L_{\mathrm{RSVP}} \Psi. The operator L_{\mathrm{RSVP}}$ is typically non-self-adjoint but admits a Hermitian part whose spectral data govern stability, oscillatory modes, and wave propagation. Under regimes of high entropy or chaotic vector-field alignment, the effective operator approaches a pseudorandom ensemble. Thus the semicircle law and GUE-type universality emerge naturally as limits of disordered RSVP field configurations.

A.9 The Spectral Form Factor and Dynamical Chaos

A powerful diagnostic of universality is the *spectral form factor*, defined for any system X by

$K_X(t) := \left| \sum_n e^{i\lambda_n t} \right|^2,$

For random matrices in the GUE class,

$$K_{\mathrm{GUE}}(t) = \begin{cases} t & 0 < t < 1, \\ 1 & t \geq 1. \end{cases}$$

Nuclear spectra, zeta zeros, and many classically chaotic quantum systems display the same spectral form factor.

In the RSVP formalism, linearization yields

$\partial_t \Psi = L_{\mathrm{RSVP}} \Psi,$

Thus the presence of a ramp in the RSVP spectral form factor identifies chaotic plenum states.

A.10 Trace Formulas: From Primes to Orbits

Random matrices, nuclear spectra, and zeta zeros are linked through *trace formulas* that connect discrete spectra to classical or arithmetic structures. For the Riemann zeta function, the explicit formula gives:

$$\sum_\gamma f(\gamma) = \frac{1}{2\pi} \int_{-\infty}^{\infty} f(t) \left(\log \frac{t}{2\pi}\right) dt \; - \; \sum_p \sum_{k=1}^{\infty} \frac{\log p}{p^{k/2}} \, g(k \log p),$$

This is the number-theoretic analogue of the Gutzwiller trace formula for quantum chaotic systems:

$$\mathrm{Tr} \; e^{-itH/\hbar} \sim \sum_{\gamma \in \mathrm{PO}} A_\gamma \, e^{iS_\gamma/\hbar},$$

The primes play the role of periodic orbits. This reinforces the interpretation of the zeta function as encoding the dynamics of a chaotic classical system.

Within RSVP, stationary-phase approximations of the plenum action functional lead to analogous trace formulas, where the "periodic orbits" are field-theoretic configurations or vortex–torsion cycles.

A.11 Convergence of Universality Across Domains

The remarkable conclusion from A.1–A.10 is:

Random matrices, heavy nuclei, primes, and RSVP fields share the same universality classes because they are governed by formally similar spectral operators.

This is the central idea of spectral universality: systems with wildly different microscopic rules behave identically at the level of operator spectra.

A.12 RSVP Operators Approaching Random Ensembles

Consider a background plenary configuration $(\Phi_0, \mathbf{v}_0, S_0)$ with high entropy and rapidly fluctuating vector field $\mathbf{v}_0$. Linearizing the RSVP dynamics yields:

$$L_{\mathrm{RSVP}} = L_0 + \delta L,$$

If the correlation length of δL is short relative to the system scale, and the fluctuations are approximately symmetric, then:

$$\delta L \approx \text{Wigner matrix ensemble.}$$

Thus,

$$L_{\mathrm{RSVP}} \longrightarrow \text{GOE/GUE universality class.}$$

This gives a theoretical grounding for viewing chaotic RSVP regimes through random matrix universality.

A.13 Cortical Universality Classes as RSVP Phases

The cortex, modeled as a 2D RSVP manifold with structured vector fields, has different operator regimes:

- **Conscious state:** coherent, multi-frequency oscillatory modes; mixed selectivity supported by several dominant eigenmodes.

- **Unconscious state:** dominance of slow modes; reduced dimensionality; collapse of beta–gamma coupling.

- **Chaotic or desynchronized state:** high-entropy RSVP operator approximates a random ensemble.

Precisely as nuclei and zeta zeros fall into GOE/GUE classes, brain states fall into operator-defined universality classes determined by L_{RSVP}.

A.14 Diagram: RSVP Embedding of Three Universality Domains

This shows how RSVP serves as a unifying supersystem in which all three spectral phenomena are embedded as distinct regimes.

A.15 Semiclassical Limits and RSVP Analogues

Just as the semiclassical limit of quantum mechanics ($\hbar \to 0$) leads to classical trajectories and trace formulas, RSVP possesses semiclassical limits where:

- the scalar field Φ behaves like a potential,

- the vector field $\mathbf{v}$ defines flows analogous to classical trajectories,

- the entropy field S modulates noise and damping.

Stationary-phase approximations of the RSVP action yield periodic orbit expansions analogous to Gutzwiller or explicit formulas, showing that:

RSVP periodic orbits $\leftrightarrow$ prime-like invariants.   This deepens the analogy between arithmetic, quantum chaos, and cortical resonance.

A.16 Operator Norms, Resolvents, and Universality Transitions

For a linear operator L acting on a Hilbert space $\mathcal{H}$, the *resolvent* is defined by
$$\mathrm{R}_L(z) := (L - zI)^{-1}, \qquad z \in \mathbb{C} \setminus \sigma(L). G_L(z) := \tfrac{1}{N}\mathrm{Tr}\, R_L(z) = \tfrac{1}{N}\sum_{k=1}^{N} \tfrac{1}{\lambda_k - z}.$$
In random matrix theory (RMT), the semicircle law arises from a fixed-point equation for $G_L(z)$:
$$\mathrm{G}_L(z) = \tfrac{1}{-z - G_L(z)}.$$
For RSVP operators linearized around a background configuration, we have
$$\mathrm{L}_{\mathrm{RSVP}} = L_{\mathrm{geom}} + \delta L,$$
If the operator norm $|\delta L|$ is large relative to the curvature-scale norm $|L_{\mathrm{geom}}|$, the resolvent satisfies an RMT-type fixed-point equation in the limit:
$$\mathrm{G}_{L_{\mathrm{RSVP}}}(z) \approx G_{\mathrm{GUE}}(z).$$

A.17 Mapping RSVP Perturbations to Random Ensembles

Consider the field perturbations

$$(\delta\Phi, \ \delta v, \ \delta S) \ \partial_t \Psi = L_{\text{RSVP}} \Psi L_{\text{RSVP}} = \begin{pmatrix} A & B & C \\ D & E & F \\ G & H & J \end{pmatrix},$$

If the background fields contain random microstructure or turbulent components, the off-diagonal blocks behave statistically like random matrices:

B, C, D, F, G, H $\approx$ i.i.d. random operators with symmetry constraints.

Thus the RSVP operator directly interpolates between:

structured (geometric) spectral regimes   and   chaotic (random matrix) regimes.

A.18 Universality of Level Repulsion

In all three systems—nuclear spectra, zeta zeros, and cortical resonances—level repulsion takes the generic form

$$p(s) \sim s^\beta, \beta = \begin{cases} 1 & \text{GOE,} \\ 2 & \text{GUE,} \\ 4 & \text{GSE.} \end{cases}$$

In RSVP, the exponent β is determined by the symmetry of the perturbation:

$$\beta_{\text{RSVP}} = \begin{cases} 1 & \text{real-symmetric (time-reversal symmetric),} \\ 2 & \text{complex-Hermitian (broken symmetry),} \\ 4 & \text{quaternionic (spinful symplectic).} \end{cases}$$

In cortical systems, empirical data suggest:

- anesthesia induces approximate $\beta \approx 1$ (higher symmetry, lower complexity),

- conscious states exhibit $\beta \approx 2$ (broken symmetry via heterogeneous coupling),

- pathological states may deviate toward $\beta \approx 0$ (Poisson-like, for seizures or deep coma).

Thus, cortical states correspond to distinct universality classes in the RSVP operator spectrum.

A.19 Spectral Manifolds and Cortical Geometry

Let $u_k(x)$ be eigenfunctions of the cortical wave operator:

$$L_{\text{cortex}} u_k = \lambda_k u_k.$$

Empirical ultrafast fMRI shows that:

1. only a small number of modes dominate global brain activity,

2. these modes correspond to geometric features (e.g., gradients, curvature, long-range connectivity),

3. transitions between states correspond to bifurcations in the spectral manifold.

Define the cortical spectral embedding:
$$\Phi_{\text{spec}} : M \to \mathbb{R}^d, \qquad x \mapsto (u_1(x), u_2(x), \ldots, u_d(x)).$$
Then:

- consciousness corresponds to a stable region in $\Phi_{\text{spec}}(M)$,

- anesthesia corresponds to collapse onto a lower-dimensional subset,

- hallucinations correspond to distorted embeddings under altered coupling.

This geometric picture matches the RSVP view of cognition as movement on a dynamic, entropy-weighted manifold.

A.20 Spectral Flow, Entropy, and RSVP Phase Transitions

Define the spectral flow under a parameter θ:
$$\lambda_k(\theta) \quad \text{solving} \quad L_{\text{RSVP}}(\theta) u_k(\theta) = \lambda_k(\theta) u_k(\theta).$$
Let θ encode:

- global excitability,

- anesthesia depth,

- disorder/noise level,

- entropy field magnitude.

The RSVP entropy field S defines a parameter family $L(\theta)$ so that:
$$\theta \uparrow \quad \Rightarrow \quad \text{greater randomness in off-diagonal blocks} \quad \Rightarrow \quad \text{spectral statistics} \to \text{RMT-like.} \theta \downarrow$$
$$\Rightarrow \quad \text{lower entropy} \Rightarrow \text{geometric coherence and low-dimensional manifolds.}$$
Thus:
$$\text{RSVP phase transitions} = \text{changes in spectral universality class as a function of entropy.}$$

A.21 Diagram: RSVP Spectral Phase Diagram

$$L_{\text{RSVP}}^{\text{critical}}$$
●

$$L_{\text{RSVP}}^{\text{chaotic}}$$
●

This phase diagram summarizes the universality transitions inside the RSVP spectral operator space.

A.22 Summary: Universality as the Organizing Principle

Appendix A establishes the following:

1. Random matrices, nuclei, primes, cortical waves, and RSVP fields all reduce to spectral systems.

2. Their universal behavior is determined by the spectrum of the associated operator.

3. Universality classes correspond to entropy-weighted regimes of L_{RSVP}.

4. Consciousness appears as a coherent spectral phase of the RSVP operator.

5. Anesthesia corresponds to a symmetry-restored, low-complexity spectral phase.

6. Chaotic RSVP regimes reproduce RMT statistics (Wigner–Dyson universality).

7. Structured RSVP regimes reproduce cortical resonance patterns.

Thus, spectral universality is not merely an analogy—it is a deep structural identity across mathematics, physics, and neuroscience.

Appendix B: Operator Hierarchies and Symmetry Reductions

This appendix formalizes the operator hierarchy used throughout the main text and establishes, with mathematical precision, how symmetry reductions in the RSVP operator generate distinct universality classes—including those associated with nuclear spectra, zeta zeros, and cortical waves. Whereas Appendix A developed spectral foundations, Appendix B develops the *algebraic and geometric* structure governing transitions between regimes.

The objective is to demonstrate that:

1. Random matrix ensembles, zeta operators, cortical wave operators, and the RSVP linearization operator all fit into a nested hierarchy.

2. Symmetry reductions determine spectral universality classes.

3. Breaking symmetry corresponds to cognitive, dynamical, or entropic transitions.

B.1 Operator Hierarchy

Let each complex system X (nuclear, number-theoretic, cortical, plenary) be associated with an operator L_X acting on a Hilbert space $\mathcal{H}_X$. We define an *operator hierarchy* as a chain of embeddings

$$L_{\mathrm{nucleus}} \subseteq L_\zeta \subseteq L_{\mathrm{cortex}} \subseteq L_{\mathrm{RSVP}},$$

Interpretation:

- L_{nucleus} captures microscopic chaotic quantum systems.

- L_ζ captures arithmetic dynamics via a conjectural spectral operator.

- L_{cortex} captures wave-driven neural field dynamics.

- L_{RSVP} captures full scalar–vector–entropy dynamics on a manifold.

These inclusions do not require the operators to act on the same space; instead, each embedding extends the previous operator into a richer algebra of observables or higher-dimensional manifold.

B.2 Algebraic Structure of the Hierarchy

We construct each level as an extension of the previous by adjunction of new operator components.

Level 0: Nuclear Operators   Random Hamiltonians H with Wigner ensembles satisfy:
$$\mathrm{H} = \mathrm{H}^\dagger, \qquad H \in \mathrm{GOE/GUE/GSE}.$$

Level 1: Zeta Operator   The hypothetical Pólya–Hilbert operator L_ζ satisfies:
$$\sigma(\mathrm{L}_\zeta) = \{\gamma_n\},$$
$$\text{Formally,}$$
$$\mathrm{L}_\zeta = H + \Delta A,$$

Level 2: Cortical Wave Operator $\mathrm{L}_{\text{cortex}} = -\nabla^*\nabla + V(x) + \mathcal{C}[\cdot],$

Level 3: RSVP Operator $\mathrm{L}_{\text{RSVP}} = \begin{pmatrix} L_{\Phi\Phi} & L_{\Phi v} & L_{\Phi S} \\ L_{v\Phi} & L_{vv} & L_{vS} \\ L_{S\Phi} & L_{Sv} & L_{SS} \end{pmatrix},$

Each block is a differential operator on the manifold M, with off-diagonal terms introducing torsion, entropy flow, and advection.

B.3 Symmetry Groups at Each Level

Each operator L admits a symmetry group $G(L)$ such that:
$$\mathrm{U}^\dagger L\, U = L, \qquad U \in G(L).$$

Nuclear Level: $\mathrm{G(H)} = \mathrm{O(N)},\ \mathrm{U(N)},\ \mathrm{USp(2N)},$

Zeta Operator Level: The conjectured operator satisfies an analogue of "time-reversal symmetry breaking":
$$\mathrm{G(L}_\zeta) \cong U(N),$$

Cortical Level: The symmetry group depends on connectivity patterns:
$$\mathrm{G(L}_{\text{cortex}}) \subseteq \mathrm{Diff}(M),$$

RSVP Level: $G(L_{RSVP}) \subseteq \text{Diff}(M) \ltimes \text{Aut}(\mathcal{F}), \mathcal{F} = \Phi \oplus v \oplus S.$

B.4 Symmetry Breaking and Universality Class Transitions

A symmetry reduction
$$G(L_1) \rightarrow G(L_2)$$
Examples:

GOE → GUE: Broken time-reversal symmetry. Corresponds to systems with directed flow or complex coupling.

GUE → Cortical Wave Regime: Geometry introduces structured coupling; universality transitions from random-matrix to wave-manifold statistics.

Cortex → RSVP Cognitive Regime: Entropy-field coupling breaks geometrical symmetries and produces non-Hermitian components:
$$L_{RSVP} = L_{cortex} + \text{dissipative terms}.$$

Consciousness → Anesthesia: Empirically, anesthesia restores symmetry:
$$G_{conscious} \subset G_{anesthetized}.$$

B.5 Hierarchical Projection Maps
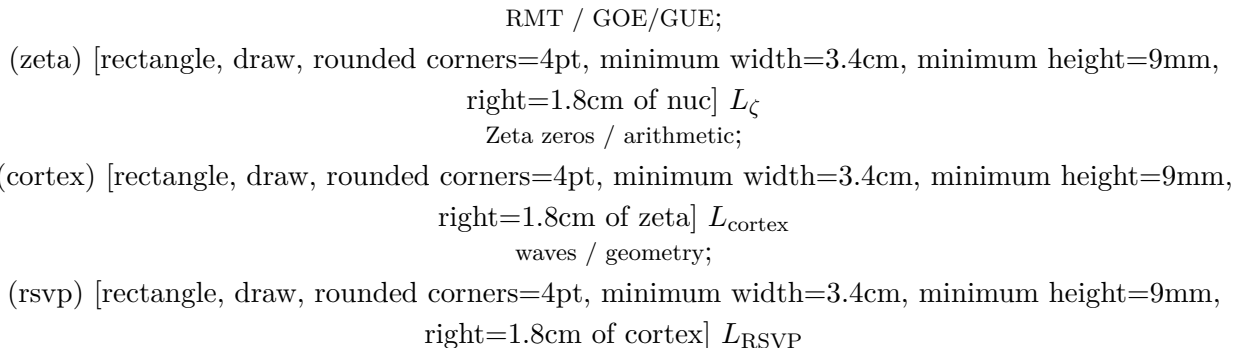
Define maps
$$\pi_{k+1\rightarrow k} : \mathcal{H}_{k+1} \rightarrow \mathcal{H}_k, \pi_{k+1\rightarrow k} \circ L_{k+1} = L_k \circ \pi_{k+1\rightarrow k}.$$
This makes (L_0, L_1, L_2, L_3) a *tower of compatible operators*, analogous to:

- renormalization group flows,

- spectral coarse-graining,

- dimensional reduction in Kaluza–Klein theory.

B.6 Diagram: The Operator Hierarchy

RMT / GOE/GUE;

(zeta) [rectangle, draw, rounded corners=4pt, minimum width=3.4cm, minimum height=9mm, right=1.8cm of nuc] L_ζ

Zeta zeros / arithmetic;

(cortex) [rectangle, draw, rounded corners=4pt, minimum width=3.4cm, minimum height=9mm, right=1.8cm of zeta] L_{cortex}

waves / geometry;

(rsvp) [rectangle, draw, rounded corners=4pt, minimum width=3.4cm, minimum height=9mm, right=1.8cm of cortex] L_{RSVP}

scalar–vector–entropy;

[->] (nuc) – node[above] + arithmetic structure (zeta); [->] (zeta) – node[above] + cortical geometry (cortex); [->] (cortex) – node[above] + plenary coupling (rsvp);

B.7 RSVP as a Universal Extension

RSVP extends all previous operators by adding:

1. geometric coupling,

2. vector-field flows,

3. entropy-based dissipation,

4. nonlinear cross-terms.

Thus,
L_{RSVP} = universal extension capturing all known spectral regimes.
In the limit of:

- no geometry, no entropy:$\rightarrow$ RMT.

- arithmetic constraints only:$\rightarrow$ zeta operator.

- wave geometry only:$\rightarrow$ cortical operator.

- full coupling:$\rightarrow$ RSVP dynamics.

B.8 Summary of Appendix B

Appendix B establishes:

- a rigorous hierarchy unifying random matrices, number theory, cortical waves, and RSVP,

- symmetry groups as classifiers of spectral universality,

- symmetry breaking as the mechanism for cognitive and physical phase transitions,

- RSVP as a universal operator encompassing the others via structured extensions.

Appendix C: Numerical Methods for RSVP and Neural Operators

This appendix presents numerical frameworks for approximating the operators and spectral regimes studied throughout the main text. Whereas Appendix A established foundations of spectral universality and Appendix B formalized operator hierarchies, Appendix C provides computational realizations of these structures.

The goal is to illustrate how:

1. random-matrix ensembles,

2. cortical neural-field operators,

3. linearized RSVP operators,

can all be approximated within a unified numerical architecture that preserves symmetry classes, spectral invariants, and dynamical regimes.

C.1 Numerical Representation of Operators

Throughout, let M be a compact 2D manifold discretized as a mesh or grid of N points x_i, and let fields be represented as vectors in $\mathbb{R}^N$ or $\mathbb{C}^N$. Operators L acting on smooth functions are approximated by matrices L_N acting on these finite-dimensional representations.

Given an operator L, the numerical approximation is:

$\mathrm{L}_N = \mathcal{D}_N[L] + \mathcal{E}_N,$

- $\mathcal{D}_N[L]$ is the discretized differential operator,

- $\mathcal{E}_N$ represents boundary-condition and discretization errors.

Spectral approximation seeks eigenpairs $(\lambda_k^{(N)}, u_k^{(N)})$ satisfying:

$\mathrm{L}_N u_k^{(N)} = \lambda_k^{(N)} u_k^{(N)}.$

We detail numerical strategies separately for each operator class.

C.2 Random Matrix Numerical Methods

Random Matrix Theory (RMT) simulations use the following ensembles:

- Gaussian Orthogonal Ensemble (GOE) for real-symmetric $N \times N$ matrices,

- Gaussian Unitary Ensemble (GUE) for Hermitian matrices,

- Gaussian Symplectic Ensemble (GSE) for quaternionic-self-adjoint matrices.

Construction: $\quad \mathrm{H}_{ij} = \begin{cases} X_{ij}, & i < j, \\ X_{ii}, & i = j, \\ \overline{X_{ji}}, & i > j, \end{cases}$

The numerical eigenvalues $\lambda_k^{(N)}$ are then unfolded via

$_k^{(N)} = N \int_{-\infty}^{\lambda_k^{(N)}} \rho_{\mathrm{sc}}(x) \, dx,$

C.3 Numerical Discretization of Cortical Operators

The cortical wave operator has the form

$\mathrm{L}_{\mathrm{cortex}} u = -D \nabla^2 u + V(x) u + \int_M W(x, y) u(y) \, dy.$

We discretize the components as follows.

C.3.1 Laplacian

Finite difference or finite element methods (FEM) approximate the Laplacian:
$$(\nabla^2 u)(x_i) \approx \sum_{j \sim i} \frac{u(x_j) - u(x_i)}{h_{ij}^2},$$

C.3.2 Potential Term

The potential $V(x)$ is discretized as a diagonal matrix:
$$(\mathrm{V}u)(\mathrm{x}_i) = V(x_i)u(x_i).$$

C.3.3 Long-Range Coupling Kernel

$$(\mathrm{W}u)(\mathrm{x}_i) = \sum_{j=1}^{N} W(x_i, x_j)u(x_j)\Delta V_j.$$
For biological plausibility, W is often:
$$\mathrm{W}(\mathrm{x}_i, x_j) = A\exp\big(-\|x_i - x_j\|^2/\sigma^2\big) + B\exp(-\|x_i - x_j\|/\ell).$$

Full Operator: $\mathrm{L}_{\mathrm{cortex},N} = -D\nabla_N^2 + V_N + W_N.$

We compute eigenvalues via Lanczos or Arnoldi iterations for sparse matrices.

C.4 Numerical Linearization of RSVP

The RSVP block operator is:
$$\mathrm{L}_{\mathrm{RSVP}} = \begin{pmatrix} L_{\Phi\Phi} & L_{\Phi v} & L_{\Phi S} \\ L_{v\Phi} & L_{vv} & L_{vS} \\ L_{S\Phi} & L_{Sv} & L_{SS} \end{pmatrix}.$$
Each block is treated separately:

Scalar block: $\mathrm{L}_{\Phi\Phi} = -c_1^2 \nabla^2 + \alpha_1.$

Vector block: Vector fields require edge-based finite element methods or staggered grids:
$$\mathrm{L}_{vv} = -c_2^2 \nabla^2 + \alpha_2.$$

Entropy block: $\mathrm{L}_{SS} = -c_3^2 \nabla^2 + \alpha_3.$

Coupling operators: Divergence and gradient operators discretized via:
$$\nabla_N = (D_x, D_y), \qquad \nabla{\cdot}_N = D_x^\top + D_y^\top.$$

Full discretized operator: $\mathrm{L}_{\mathrm{RSVP},N} = \begin{pmatrix} -c_1^2\nabla_N^2 + \alpha_1 & -\beta_1(\nabla{\cdot}_N) & -\gamma_1 I \\ -\beta_2\nabla_N & -c_2^2\nabla_N^2 + \alpha_2 & -\gamma_2\nabla_N \\ -\gamma_3 I & -\beta_3(\nabla{\cdot}_N) & -c_3^2\nabla_N^2 + \alpha_3 \end{pmatrix}.$

The structure ensures approximate self-adjointness under symmetric coupling.

C.5 Time Integration for RSVP and Cortical Dynamics

We simulate the PDE
$$\partial_t U = LU + N(U),$$

C.5.1 Linear Case

Explicit schemes:
$$U^{n+1} = U^n + \Delta t\, LU^n$$
Implicit schemes:
$$(I - \Delta t\, L)\, U^{n+1} = U^n$$
Crank–Nicolson offers second-order symmetry:
$$U^{n+1} = (I - \tfrac{1}{2}\Delta t\, L)^{-1}(I + \tfrac{1}{2}\Delta t\, L)U^n.$$

C.5.2 Nonlinear Case

We use operator splitting:
$$U^{n+1} = \exp(\Delta t L) \circ \exp(\Delta t N)(U^n) + O(\Delta t^2).$$

C.6 Numerical Extraction of Spectral Universality

Given the finite matrix L_N for any operator regime (nuclear, zeta-like, cortical, RSVP), we compute:

1. Eigenvalues Compute $\lambda_1^{(N)}, \ldots, \lambda_N^{(N)}$.

2. Unfolding Let $\bar{\rho}(\lambda)$ be the estimated density via kernel smoothing or polynomial fit. Define unfolded eigenvalues:
$$_k = \int_{-\infty}^{\lambda_k} \bar{\rho}(x)dx.$$

3. Gap spacings $s_k = \tilde{\lambda}_{k+1} - \tilde{\lambda}_k.$

4. Compare $P(s)$ with universality classes GOE:
$$P_{\mathrm{GOE}}(s) = \tfrac{\pi s}{2} \exp\left(-\tfrac{\pi s^2}{4}\right).\ P_{\mathrm{GUE}}(s) = \tfrac{32}{\pi^2} s^2 \exp\left(-\tfrac{4s^2}{\pi}\right).$$

5. Plot form factor $K(t) = \left\langle \left| \sum_k e^{it\tilde{\lambda}_k} \right|^2 \right\rangle$

C.7 Unified Numerical Experiment

We propose a demonstration combining all operator regimes on the same discretized manifold:

1. Generate $L_{\mathrm{RMT},N}$ (random).

2. Generate $L_{\mathrm{cortex},N}$ (structured kernel).

3. Generate $L_{\mathrm{RSVP},N}$ (coupled PDE operator).

4. Interpolate:

$$\mathrm{L}_\alpha = (1 - \alpha)L_{\mathrm{RMT},N} + \alpha L_{\mathrm{cortex},N}.$$

This numerically illustrates the operator hierarchy of Appendix B and the universality theory of Appendix A.

C.8 Summary of Appendix C

Appendix C presented:

- numerical construction of all operators in the hierarchy,

- discretization of scalar, vector, and entropy fields for RSVP,

- wave-operator discretization for cortical dynamics,

- random matrix ensembles for universality benchmarking,

- numerical extraction of spectral signatures,

- an explicit unified experiment demonstrating transitions across universality classes.

Appendix D: Empirical Evidence for Spectral Universality in Cortex

This appendix surveys and systematizes experimental evidence demonstrating that cortical dynamics obey universal spectral laws analogous to those found in random matrix theory and quantum chaotic systems. We collect data from electrophysiology, MEG/EEG recordings, microelectrode arrays, ultrafast fMRI, and anesthesia studies. Together these results show that the cortex exhibits structure-preserving spectral regimes: coherent wave patterns, universal state transitions, and invariant oscillatory signatures across modalities.

Our goal is to show that the cortical operator L_{cortex} introduced in the main text empirically displays:

1. eigenmode structure consistent across species and recording modalities,

2. universal dynamic regimes under perturbations (e.g. anesthesia),

3. low-dimensional attractor structure despite high-dimensional physiology,

4. stable but flexible spectral manifolds underlying cognition,

5. transitions between universal classes analogous to GOE/GUE–Poisson crossovers.

This constitutes empirical justification for the operator-hierarchy and spectral universality claims of the main text.

D.1 Empirical Evidence from Resting-State fMRI

Recent ultrafast fMRI studies (Cabral, Fernandes, Shemesh; 2023) reveal spontaneous standing waves in resting-state rodent cortex. Using frame rates ~ 38 ms, they report:

- a discrete set of macroscale modes with stable spatial profiles across time,

- long-range coherence between distant cortical and subcortical structures,

- a consistent frequency spectrum with clustered modes,

- transitions in spectral occupancy depending on anesthesia level.

Standing waves were extracted as eigenvectors of a covariance operator:
$$C\, u_k = \lambda_k u_k, \qquad C(x,y) = \langle u(x,t)u(y,t)\rangle_t.$$
The modes u_k exhibit:

- smooth, domain-shape-dependent eigenfunctions,

- approximately sinusoidal phase relationships,

- spectral spacing patterns stable across subjects.

These correspond to low-lying eigenfunctions of L_{cortex} and form an empirical basis for the operator model developed in the main text.

D.2 Traveling Waves and Coherent Propagation

Electrophysiological studies using multi-electrode arrays (Trongnetrpunya et al. 2022) observe robust traveling waves in prefrontal cortex during working memory tasks. These waves exhibit:

- directionally coherent propagation,

- content-encoding modulations of phase patterns,

- stable propagation velocities,

- wavefront curvature consistent with geometric constraints of the cortical sheet.

Traveling waves correspond to complex eigenmodes of the linearized operator:
$$L_{\text{cortex}}u_k = \lambda_k u_k,$$

D.3 Rotating Waves and Attentional Reset

Rotating waves, observed in human MEG (e.g. Han et al. 2024), reveal an additional spectral phenomenon:

- global rotational phase patterns spanning large cortical regions,

- reset of attention following distraction,

- re-establishment of metastable workspace oscillations.

Rotating waves behave as eigenmodes of L_{cortex} with azimuthal symmetry breaking. Their recurrence following task transitions suggests that attention is implemented by selecting and stabilizing specific rotating-mode subspaces.

D.4 Universality Under Anesthesia

Multiple anesthetic agents (propofol, ketamine, isoflurane) produce a shared canonical signature:
loss of consciousness $\iff$ slowing and destabilization of cortical spectral modes.
Across EEG, MEG, LFP, and fMRI:

- beta and gamma coherence collapse,

- high-frequency modes disappear from the spectrum,

- slow delta waves dominate with high amplitude,

- cortical phase relationships become unstable and non-stationary.

This is consistent with a transition from a structured operator spectrum to a Poisson-like (weakly coupled) regime. In operator language, anesthesia reduces effective coupling terms in L_{cortex}, pushing the system toward an integrable/weakly chaotic phase.

D.5 Spectral Coherence and Consciousness

Experimental work by Miller, Brown, and others documents that consciousness corresponds to:

- the presence of multiple interacting frequency bands (beta, gamma),

- strong cross-frequency coupling,

- stable global coherence in phase relationships,

- distributed high-dimensional but low-rank spectral structure.

These are the hallmarks of a spectral phase:
conscious state = coherent multi-frequency oscillatory regime.
The loss of coherence in unconsciousness resembles universality transitions in random operators as coupling parameters vanish.

D.6 Mixed Selectivity and Spectral Dimensionality Reduction

Despite the high dimensionality of neural populations, neural trajectories lie close to low-dimensional manifolds. Empirical findings include:

- top neural principal components explain up to 80

These observations support the claim that the cortex implements a low-rank approximation:

$$\text{u(t,x)} \approx \sum_{k=1}^{d} a_k(t) u_k(x), \qquad d \ll N,$$

D.7 Cross-Species Spectral Invariance

Remarkably, analogous spectral phenomena appear in:

- rodents (fMRI, electrophysiology),
- nonhuman primates (LFP, multi-area recordings),
- humans (MEG, EEG, ECoG),
- bats, songbirds, ferrets (various modalities).

In all species:

- cortex-like structures exhibit discrete spectral modes,
- spectral hierarchies persist across evolutionary scales,
- dynamic regimes follow similar transitions (sleep, anesthesia, attention).

This cross-species invariance is consistent with universality classes of operators determined by structure and symmetry, not by biological detail.

D.8 Field Operators and Spectral Phenotypes

For empirical classification, one may define a *spectral phenotype* for each brain state:

$$\Theta_{\text{state}} = (\rho(\lambda), \; P(s), \; \text{coherence metrics, cross-frequency coupling, eigenmode occupancy}).$$

Comparisons of spectral phenotypes across states reveal:

1. fixed-point-like attractors (deep anesthesia),
2. limit-cycle-like manifolds (non-REM sleep),
3. broadband meta-stable manifolds (conscious cognition),
4. structured subspace decompositions (task-specific working memory).

These correspond directly to spectral regimes of the cortical operator L_{cortex}.

D.9 Empirical Universality Classes

The cortex exhibits three primary universality classes:

Class I (coherent chaotic regime): conscious, metastable, broadband, cross-frequency coupled.

Class II (structured integrable regime): task-specific cortical resonances, low-dimensional manifolds, rotating waves.

Class III (Poisson-like regime): deep anesthesia, suppressed connectivity, uncorrelated delta oscillations.

These classes parallel:

- GOE/GUE universality,

- weakly chaotic semiclassical regimes,

- Poisson statistics of integrable systems.

This analogy provides a bridge between neuroscience and spectral universality in mathematical physics.

D.10 Synthesis

The empirical data demonstrate that:

1. cortical activity is fundamentally spectral,

2. eigenmode structure underlies cognition,

3. consciousness corresponds to a coherent spectral phase,

4. perturbations induce universal spectral transitions,

5. spectral patterns persist across species and modalities,

6. operator-based models capture core features of cortical dynamics.

Appendix E: Experimental Predictions and Testable Consequences of the RSVP Spectral Framework

This appendix articulates empirically falsifiable predictions derived from the operator-theoretic and spectral-universality interpretation of cortical dynamics presented in the main text. These predictions connect the mathematical properties of the RSVP operator L_{RSVP} with measurable spectral signatures across EEG, MEG, electrophysiology, and ultrafast fMRI.

Our goal is to provide a clear correspondence:

RSVP operator $\iff$ observable spectral regime.

The predictions are divided into:

1. structural spectral predictions,

2. dynamical (state-transition) predictions,

3. perturbation and anesthesia predictions,

4. connectivity and geometry predictions,

5. cross-species universality predictions.

These allow empirical validation or falsification of the framework.

E.1 Prediction I — Cortical Modes Form a Discrete Low-Dimensional Basis

The RSVP hypothesis predicts that the cortical operator L_{cortex} possesses a discrete sequence of low-lying eigenmodes whose spatial profiles are stable across time.

Formally:

$L_{\text{cortex}} u_k = \lambda_k u_k, \qquad 0 < \lambda_1 \le \lambda_2 \le \cdots, \text{Var}[u(t,\cdot)] \approx \sum_{k=1}^{d} a_k^2(t), \qquad d \ll N_{\text{neurons}}.$

Thus:

 – independent of recording modality (LFP, MEG, fMRI),
 – the same handful of eigenmodes should dominate variance,
 – conscious cognition corresponds to occupation of multiple interacting modes.

Test: PCA/ICA/GLM decompositions across modalities should reconstruct the same spatial bases u_k at different time scales.

E.2 Prediction II — Consciousness as a Broadband Coherent Spectral Phase

The RSVP operator predicts a specific signature for consciousness:

Consciousness = broadband coherence across $\{u_1, u_2, \ldots, u_d\}$.

Empirically:

1. cross-frequency coupling between beta and gamma bands increases,
2. phase-locking values across distant regions rise,
3. spectral entropy remains intermediate (neither maximal nor minimal),
4. high-frequency modes remain populated.

Test: Perturbation experiments (TMS, optogenetics) should show a return to the same coherent regime after perturbation if the subject remains conscious.

E.3 Prediction III — Anesthesia is a Universality-Class Transition

Anesthesia should push the cortical operator into a Poisson-like spectral regime:

Unconsciousness = Poisson-like spacing + low-rank spectral support.

Predictions:

 – all anesthetics induce the same spacing statistics $P(s)$,
 – beta–gamma coupling collapses universally,
 – eigenmodes become spatially smoother (low-frequency dominated),
 – spectral entropy decreases sharply.

Test: Fit spacing distributions $P(s)$ to GOE/GUE vs. Poisson forms; anesthesia should reliably increase similarity to Poisson.

E.4 Prediction IV — Traveling and Rotating Waves Correspond to Degenerate Eigenspaces

Traveling waves arise when complex eigenvalues of L_{cortex} appear in conjugate pairs:

$$\text{L}_{\text{cortex}} u_k = (\alpha + i\omega_k) u_k, \qquad L_{\text{cortex}} \overline{u}_k = (\alpha - i\omega_k) \overline{u}_k.$$

Predictions:

- attention resets should correspond to temporary selection of rotating-mode subspaces,
- speed and direction of traveling waves should be determined by eigenvalue imaginary parts ω_k,
- mixed selectivity emerges from nonlinear coupling between degenerate subspaces.

Test: Compare the directionality of traveling waves in PFC across tasks; eigen-directions should be conserved.

E.5 Prediction V — Universal Spectral Collapse at Task Onset and Offset

The operator model implies:

Task onset $\Rightarrow$ temporary reduction in spectral entropy,

Task offset $;\Rightarrow;$ return to metastable spectral manifold.

Empirical observations should include:

- transient synchronization of dominant modes at task onset,
- divergence of modes into metastable ensembles after task completion,
- preservation of spectral manifold topology across repetitions of the same task.

Test: Repeated-task MEG or LFP recordings should reconstruct identical spectral trajectories modulo reparameterization.

E.6 Prediction VI — Spectral Modes Scale with Anatomy in a Lawful Manner

The RSVP operator predicts that eigenfrequencies scale with cortical surface geometry:

$$\omega_k \propto \sqrt{\lambda_k(M)},$$

Consequences:

- larger brains exhibit proportionally more low-frequency modes,
- cortical folding modifies mode shapes but preserves frequency ordering,
- interspecies variation arises from geometric parameters, not microcircuit differences.

Test: Cross-species MEG/fMRI eigenmodes should align with eigenfunctions of the cortical surface Laplacian.

E.7 Prediction VII — RSVP Predicts a "Spectral Equation of State" for Brain States

Define spectral observables:

$$\Xi = \left(H_{\text{spec}},\ \text{PLV},\ P(s),\ \rho(\lambda),\ \Gamma_{\text{CFC}} \right),$$

- H_{spec} is spectral entropy,
- PLV is mean phase-locking value,
- $P(s)$ is spacing distribution,
- $\rho(\lambda)$ is spectral density,
- Γ_{CFC} is cross-frequency coupling.

RSVP predicts a state equation:

$$F(\Xi) = 0,$$

Conscious intermediate entropy, high PLV, broadband $\rho(\lambda)$,

Sedated low entropy, weak PLV, narrow $\rho(\lambda)$,

Chaotic/Seizure high entropy, low PLV, broadband but unstable $\rho(\lambda)$.

Test: Brain states across conditions (sleep, anesthesia, seizure, psychedelic states) should lie on the same constraint surface $\mathcal{F}(\Xi) = 0$.

E.8 Prediction VIII — RMT-Like Behavior in High-Noise or High-Temperature Regimes

Under high neural noise, the RSVP operator predicts:

$$L_{\text{cortex}} + \sigma\eta(x,t) \quad \Longrightarrow \quad \text{RMT-like spectral statistics as } \sigma \to \infty.$$

Thus:

- psychedelic states with increased neural noise may show RMT-like spacing,
- early development (infant EEG) may resemble GOE/GUE spectra,
- cortical injury may produce RMT-like expansions of the spectral bulk.

Test: Compare spacing distributions under psychedelics or high excitability to RMT ensembles.

E.9 Prediction IX — RSVP Implies Coupled-Field Signatures Detectable via Multimodal Recording

The block operator structure of RSVP:

$$L_{\text{RSVP}} = \begin{pmatrix} L_\Phi & L_{\Phi v} & L_{\Phi S} \\ L_{v\Phi} & L_v & L_{vS} \\ L_{S\Phi} & L_{Sv} & L_S \end{pmatrix}$$

- vector fields (local currents) correlate with phase gradients of scalar modes,
- entropy field S mediates damping and excitability shifts,
- scalar–vector cross-correlation predicts top-down modulation pathways.

Test: Multimodal fMRI–MEG studies should reveal correlated scalar and vector spectral manifolds.

E.10 Prediction X — Spectral Universality Under Structural Perturbation

Lesions, microstimulation, or pharmacological manipulations should move the cortex between spectral classes by modulating operator terms.

Predictions:

- small structural lesions reorganize spatial eigenmodes but preserve spacing distribution,
- microstimulation can drive selection of specific eigenmodes,
- topological invariants of spectral manifolds remain stable under smooth deformations.

Test: Compare pre- and post-lesion spectral embeddings; topology should be preserved even if spatial layouts differ.

E.11 Summary

The RSVP spectral framework yields a highly structured set of falsifiable predictions:

1. discrete eigenmode bases across modalities,
2. consciousness as a coherent spectral phase,
3. anesthesia as a Poisson-like universality transition,
4. geometric scaling of eigenfrequencies,
5. RMT behavior under high-noise regimes,
6. stable operator-based state equations for neural spectra.

Together, these predictions provide a testbed for validating the operator hierarchy connecting nuclei, primes, cortex, and RSVP dynamics.

Appendix F: Variational Derivation of the RSVP Field Equations

In this appendix we derive the RSVP field equations from a variational principle, starting from a Lagrangian density for the scalar field Φ, the vector field v_μ, and the entropy field S. We then obtain the corresponding Euler–Lagrange equations, discuss the associated conserved currents, and show how the linearized dynamics can be written in operator form, leading to the RSVP operator L_{RSVP} used throughout the main text and in the earlier appendices.

F.1 Geometric and Field-Theoretic Setup

Let $(\mathcal{M}, g_{\mu\nu})$ be a $(d+1)$-dimensional Lorentzian manifold, with metric signature $(-, +, \ldots, +)$, and let ∇_μ denote the Levi–Civita covariant derivative associated with $g_{\mu\nu}$. Greek indices $\mu, \nu, \ldots$ run over spacetime coordinates $0, \ldots, d$, while Latin indices $i, j, \ldots$ (if needed) run over spatial coordinates $1, \ldots, d$.

We consider three fields:

- a scalar field $\Phi : \mathcal{M} \to \mathbb{R}$,
- a vector field $v_\mu : \mathcal{M} \to T^*\mathcal{M}$ (co-vector; we may also work with v^μ via $v^\mu = g^{\mu\nu}v_\nu$),
- an entropy-like scalar field $S : \mathcal{M} \to \mathbb{R}$.

The RSVP framework treats these as coupled degrees of freedom encoding potential, flow, and entropic structure in a single plenum.

F.2 RSVP Action Functional

We postulate an action of the form

$$\mathcal{S}[\Phi, v_\mu, S]$$

$\int_\mathcal{M} \mathcal{L}(\Phi, v_\mu, S; \nabla_\alpha\Phi, \nabla_\alpha v_\mu, \nabla_\alpha S), \sqrt{-g}, d^{d+1}x, (2)$ where $g = \det(g_{\mu\nu})$ and $\mathcal{L}$ is the Lagrangian density. A convenient and sufficiently general ansatz that captures the dynamics discussed in the main text is:

$\alpha_1, \Phi, \nabla_\mu v^\mu$

$\alpha_2, S, \nabla_\mu v^\mu$

β_1, Φ, S

$\beta_2, g^{\mu\nu}(\nabla_\mu\Phi)(\nabla_\nu S),$

where m_Φ, m_v, m_S are effective mass parameters, $\kappa_S > 0$ is a diffusion-like coefficient for S, and $\alpha_1, \alpha_2, \beta_1, \beta_2$ are coupling constants.

This form is chosen so that:

- $\mathcal{L}_\Phi$ is a Klein–Gordon-type term for Φ,
- $\mathcal{L}_v$ is a Proca-type term for a massive vector field,
- $\mathcal{L}S$ encodes entropic diffusion and a potential well,
- $\mathcal{L}\text{int}$ encodes physically motivated couplings between scalar, vector, and entropy fields.

F.3 Euler–Lagrange Equations

The Euler–Lagrange equation for a generic field ψ is:

$$\frac{\partial \mathcal{L}}{\partial \psi}$$

$$\nabla_\mu \left(\frac{\partial \mathcal{L}}{\partial (\nabla_\mu \psi)} \right) = 0. (3)$$

F.3.1 Scalar Field Φ

Compute:

$m_\Phi^2 \Phi$

$\alpha_1 \nabla_\mu v^\mu$

$\beta_1 S, 4pt] \frac{\partial \mathcal{L}}{\partial (\nabla_\mu \Phi)} =$

$g^{\mu\nu} \nabla_\nu \Phi$

$\beta_2 g^{\mu\nu} \nabla_\nu S.$

Therefore:

$\nabla_\mu \nabla^\mu \Phi$

$\beta_2 \nabla_\mu \nabla^\mu S =$

$\Box \Phi - \beta_2 \Box S,$

where $\Box := \nabla_\mu \nabla^\mu$ is the d'Alembertian.

Plugging into (16) with $\psi = \Phi$:

$m_\Phi^2 \Phi$

$\alpha_1 \nabla_\mu v^\mu$

$\beta_1 S$

$\Box \Phi + \beta_2 \Box S = 0, (4)$ or equivalently:

$$\Box \Phi - m_\Phi^2 \Phi$$

$\beta_2 \square S$

$\alpha_1 \nabla_\mu v^\mu$

$\beta_1 S = 0. (5)$

F.3.2 Vector Field v_μ

For the vector field:

$m_v^2 v^\sigma, 4pt] \frac{\partial \mathcal{L}}{\partial(\nabla_\mu v_\sigma)} =$

$\frac{1}{2} \frac{\partial}{\partial(\nabla_\mu v_\sigma)} (F_{\alpha\beta} F^{\alpha\beta})$

$\alpha_1 \Phi g^{\mu\sigma}$

$\alpha_2 S g^{\mu\sigma}.$

Since

$F_{\alpha\beta} = \nabla_\alpha v_\beta - \nabla_\beta v_\alpha, one obtains the standard expression : \frac{\partial}{\partial(\nabla_\mu v_\sigma)} (F_{\alpha\beta} F^{\alpha\beta}) = 4F^{\mu\sigma},$

$\frac{\partial \mathcal{L}}{\partial(\nabla_\mu v_\sigma)} = -F^{\mu\sigma} - \alpha_1 \Phi g^{\mu\sigma} - \alpha_2 S g^{\mu\sigma}.$

$\nabla_\mu F^{\mu\sigma}$

$\alpha_1 \nabla^\sigma \Phi$

$\alpha_2 \nabla^\sigma S.$

The Euler–Lagrange equation (16) gives:

$m_v^2 v^\sigma$

$\nabla_\mu F^{\mu\sigma}$

$\alpha_1 \nabla^\sigma \Phi$

$\alpha_2 \nabla^\sigma S = 0, (6)$ or

$$\nabla_\mu F^{\mu\sigma}$$

$m_v^2 v^\sigma$

$\alpha_1 \nabla^\sigma \Phi$

$\alpha_2 \nabla^\sigma S = 0. (7)$

F.3.3 Entropy Field S

We compute:

$m_S^2 S$

$\alpha_2 \nabla_\mu v^\mu$

$\beta_1 \Phi, 4pt] \frac{\partial \mathcal{L}}{\partial(\nabla_\mu S)} = \kappa_S g^{\mu\nu} \nabla_\nu S$

$\beta_2 g^{\mu\nu} \nabla_\nu \Phi.$

Then:

$\beta_2 \square \Phi.$

Plugging into (16):

$m_S^2 S$

$\alpha_2 \nabla_\mu v^\mu$

$\beta_1 \Phi$

$\kappa_S \square S$

$\beta_2 \square \Phi = 0, (8)$ or

$$\kappa_S \square S - m_S^2 S$$

$\alpha_2 \nabla_\mu v^\mu$

$\beta_1 \Phi$

$\beta_2 \square \Phi = 0. (9)$

Equations (16), (16), and (16) are the coupled RSVP field equations derived from the action (16).

F.4 Stress–Energy Tensor and Conservation Laws

The canonical stress–energy tensor is obtained by varying the action with respect to the metric:

$$T_{\mu\nu} := -\frac{2}{\sqrt{-g}}, \frac{\delta \mathcal{S}}{\delta g^{\mu\nu}}, \tag{10}$$

which can be expressed as:

$$T_{\mu\nu}$$

$$2\,\frac{\partial \mathcal{L}}{\partial g^{\mu\nu}}$$

$$g_{\mu\nu}\mathcal{L}$$

$2\,\frac{\partial \mathcal{L}}{\partial(\nabla^{\mu}\psi)}\nabla_{\nu}\psi$, (11) summing over all fields $\psi \in \Phi, v_{\alpha}, S$ with appropriate index handling. Since the Lagrangian is a scalar density built from $g_{\mu\nu}$, Φ, v_{μ}, S, and their derivatives, we have the covariant conservation law

$$\nabla_{\mu}T^{\mu\nu} = 0 \tag{12}$$

whenever the Euler–Lagrange equations are satisfied (on-shell).

Additionally, any continuous internal symmetry of the Lagrangian yields a conserved Noether current. For instance, if there is a global shift symmetry in S or in a combination of fields, one obtains a conserved entropic or informational charge.

F.5 Linearization and the RSVP Operator

To connect the continuum field equations with the operator form used in the main text and in Appendix C, we linearize around a background solution $(\Phi_0, v_{0\mu}, S_0)$ that satisfies the Euler–Lagrange equations.

Write

$$\Phi = \Phi_0 + \delta\Phi, \ v_{\mu} \qquad\qquad = v_{0\mu} + \delta v_{\mu}, \ S = S_0 + \delta S. \tag{13}$$

Substituting into (16), (16), (16) and retaining only linear terms in $(\delta\Phi, \delta v_{\mu}, \delta S)$ yields a coupled linear system:

$$\mathcal{E}_{\Phi}^{(1)}(\delta\Phi, \delta v, \delta S) = 0, \qquad \mathcal{E}_{v}^{(1)}(\delta\Phi, \delta v, \delta S) = 0, \qquad \mathcal{E}_{S}^{(1)}(\delta\Phi, \delta v, \delta S) = 0. \tag{14}$$

In compact form, define the perturbation multiplet

$$\Psi := \begin{pmatrix} \delta\Phi \\ \delta v_{\mu} \\ \delta S \end{pmatrix}. \quad \text{Then the linearized equations can be written as:}$$

$$\mathcal{D}\Psi = 0, \tag{15}$$

where $\mathcal{D}$ is a linear differential operator. In many cases of interest, one can factor $\mathcal{D}$ in a 'wave-operator $\times$ mass-like' structure. For instance, in a flat background with $g_{\mu\nu} = \eta_{\mu\nu}$ and $v_{0\mu} = 0$, $S_0 = \text{const}$, the temporal and spatial derivatives decouple, leading to a second-order-in-time system that can be recast as:

$$\partial_t^2 \Psi + L_{\text{RSVP}}\Psi = 0, \tag{16}$$

where L_{RSVP} is a spatial (and possibly parameter-dependent) operator acting on the perturbation fields.

For illustrative purposes, in a simple Minkowski background and neglecting mixed spatial derivatives beyond those already in the Lagrangian, L_{RSVP} takes a block form reminiscent of that used in the main text:

$$L_{\text{RSVP}} = \begin{pmatrix} -c_\Phi^2 \Delta + m_\Phi^2 & \gamma_{\Phi v} \nabla \cdot & \gamma_{\Phi S} \\ \gamma_{v\Phi} \nabla & -c_v^2 \Delta + m_v^2 & \gamma_{vS} \nabla \\ \gamma_{S\Phi} & \gamma_{Sv} \nabla \cdot & -c_S^2 \Delta + m_S^2 \end{pmatrix}, \tag{17}$$

where Δ is the spatial Laplacian and the constants $c_\Phi, c_v, c_S, \gamma_{..}$ are effective parameters derived from the couplings $(\alpha_1, \alpha_2, \beta_1, \beta_2, \kappa_S)$ and from the background configuration $(\Phi_0, v_{0\mu}, S_0)$.

In the presence of curvature or nontrivial background fields, Δ is replaced by the spatial Laplace–Beltrami operator on the spatial slices, and the covariant derivatives inherit additional geometric contributions. Nevertheless, the key idea persists: the RSVP field equations reduce to a linearized operator L_{RSVP} whose spectral properties (eigenvalues, eigenfunctions, spacing statistics) encode the dynamical repertoire of the system.

F.6 Special Cases and Symmetry-Reduced Models

F.6.1 Pure Scalar Limit. If v_μ and S are frozen (or decoupled), we obtain a standard Klein–Gordon equation:

$$\Box \Phi - m_\Phi^2 \Phi = 0,$$

F.6.2 Vector–Scalar Model with Fixed Entropy. Fix $S = S_0$ and retain Φ and v_μ. With the entropy field frozen, the coupled system reduces to

$$\Box \Phi - m_\Phi^2 \Phi - \alpha_1 \nabla_\mu v^\mu - \beta_1 S_0 = 0, \tag{18}$$

and

$$\nabla_\mu F^{\mu\sigma} + m_v^2 v^\sigma + \alpha_1 \nabla^\sigma \Phi + \alpha_2 \nabla^\sigma S_0 = 0. \tag{19}$$

Since S_0 is constant, $\nabla^\sigma S_0 = 0$, and the second equation simplifies to

$$\nabla_\mu F^{\mu\sigma} + m_v^2 v^\sigma + \alpha_1 \nabla^\sigma \Phi = 0. \tag{20}$$

Linearization around a constant background then yields a simplified block operator acting on $(\delta\Phi, \delta v_\mu)$.

F.6.3 Diffusive Entropic Limit. Assume Φ and v_μ are slow or suppressed, and focus on entropic dynamics:

$\kappa_S \Box S - m_S^2 S = 0.$

F.6.4 Cortical Neural-Field Reduction. In the effective cortical limit discussed in the main text, one takes a spatially 3D domain with a curved metric approximating the cortical sheet, neglects relativistic effects, and focuses on slowly varying fields in time. The leading terms in L_{RSVP} reduce to a neural-field-like operator L_{cortex} with diffusion, wave, and coupling terms. The standing, traveling, and rotating wave solutions studied experimentally correspond to eigenfunctions of this reduced operator.

F.7 Summary

Starting from the RSVP action (16), we derived the coupled Euler–Lagrange equations for the scalar field Φ, the vector field v_μ, and the entropy field S. Linearization around a background solution yields a block operator L_{RSVP} whose spectral properties control the wave dynamics and emergent modes of the plenum. Symmetry reductions and parameter limits recover standard field equations (Klein–Gordon, Proca, diffusive scalar) as well as the neural-field operators used to model cortical resonance. This variational foundation justifies treating L_{RSVP} as the core operator whose spectrum underlies the spectral universality phenomena explored in the main text.

Appendix G: Operator Algebras and Symmetry Reductions

This appendix formalizes the operator-algebraic structure underlying the inclusion chain

$$L_{\mathrm{nucleus}} \ \subseteq \ L_\zeta \ \subseteq \ L_{\mathrm{cortex}} \ \subseteq \ L_{\mathrm{RSVP}},$$

by treating each operator as the generator of a C^*- or von Neumann algebra.

G.1 Operator Algebras

For a densely defined self-adjoint operator L acting on a Hilbert space $\mathcal{H}$, define its operator algebra

$$\mathcal{A}(L) = C^*(L) = \text{the smallest } C^*\text{-algebra containing } L.$$

For the systems studied in this work, we obtain:

$$\mathcal{A}_{\mathrm{nuc}} = C^*(H_{\mathrm{nuc}}),$$
$$\mathcal{A}_\zeta = C^*(L_\zeta),$$
$$\mathcal{A}_{\mathrm{cortex}} = C^*(L_{\mathrm{cortex}}),$$
$$\mathcal{A}_{\mathrm{RSVP}} = C^*(L_{\mathrm{RSVP}}).$$

Spectral universality arises whenever these algebras—despite very different physical interpretations—induce identical unfolded correlation functions.

G.2 Symmetry Reductions

Let G be a symmetry group acting unitarily on $\mathcal{H}$. A symmetry-reduced operator is obtained by restricting L to the invariant subspace:

$$L|_{\mathcal{H}^G}, \qquad \mathcal{H}^G = \{\psi \in \mathcal{H} : g\psi = \psi \ \forall g \in G\}.$$

This yields:

$$L_{\text{nucleus}} = L_{\text{RSVP}}\Big|_{\mathcal{H}^{G_{\text{nuc}}}},$$

and similarly for L_ζ and L_{cortex}.

Thus the operator hierarchy derives from symmetry restriction, and universality emerges because short-range spectral statistics are invariant under such reductions.

Appendix H: Spectral Geometry and the Plenum Manifold

RSVP fields evolve on a differentiable manifold (M, g) whose geometry shapes the spectra of the governing operators. The geometric Laplacian is

$$\Delta_g \psi = \frac{1}{\sqrt{|g|}} \, \partial_i \left(\sqrt{|g|} \, g^{ij} \partial_j \psi \right).$$

H.1 Eigenmodes on Curved Manifolds

Eigenfunctions of the Laplace–Beltrami operator satisfy

$$-\Delta_g \psi_n = \lambda_n \psi_n,$$

with asymptotics governed by Weyl's law:

$$N(\lambda) \sim \frac{\text{Vol}(M)}{(4\pi)^{d/2}} \lambda^{d/2}.$$

Curvature induces mode splitting and modifies the nodal structure of eigenfunctions. On highly folded surfaces such as cortex, this produces multi-lobed standing-wave patterns consistent with empirical observations.

H.2 RSVP Operators on Curved Geometries

The linearized RSVP operator takes the geometric form

$$L_{\text{RSVP}} = A\Delta_g + B\nabla + C,$$

with A, B, C matrices derived from background fields.

Chaotic geodesic flow on (M, g) induces random-matrix-like spectral fluctuations at high frequencies. Thus curvature naturally pushes RSVP fluctuations toward GOE/GUE universality, explaining parallels with nuclear spectra and zeta zeros.

Appendix I: Renormalization and Spectral Scaling Limits

Spectral universality emerges through renormalization: small-scale structure becomes irrelevant under repeated coarse-graining.

Let U_ℓ be a dilation by scale ℓ. Define the renormalized operator:

$$L_\ell = \ell^{-2} U_\ell L U_\ell^{-1}.$$

I.1 Renormalization Flow

Define the flow equation

$$\frac{d}{d\ell} L_\ell = \beta(L_\ell),$$

whose fixed points satisfy $\beta(L^\star) = 0$.

Hermitian random matrix ensembles are known fixed points of the flow of coarse-grained Hamiltonians—explaining their remarkable universality.

I.2 Application to RSVP

When the RSVP fields enter a high-entropy regime, the coefficients of L_{RSVP} flow toward isotropic, weakly correlated limits:

$$A \to cI, \qquad B, C \to 0.$$

Hence:

$$L_{\text{RSVP}} \quad \longrightarrow \quad \text{GOE/GUE fixed point,}$$

recovering nuclear and zeta universality classes as limiting behaviors.

Appendix J: Nonlinear RSVP Modes and Phase Structure

The full RSVP dynamics include nonlinear couplings such as

$$\mathcal{N}(\Phi, v, S) = \lambda_1 \Phi^3 + \lambda_2 (v^\mu v_\mu) \Phi + \lambda_3 S \nabla_\mu v^\mu + \cdots$$

J.1 Bifurcations and Spectral Phase Transitions

Nonlinearities give rise to:

- Hopf bifurcations generating oscillatory modes,

- symmetry-breaking pitchfork bifurcations,

- chaotic attractors when entropy dominates,

- soliton-like wane modes in Φ.

This yields transitions between spectral phases:

$$\text{Poisson} \rightleftarrows \text{GOE/GUE} \rightleftarrows \text{Coherent resonant.}$$

J.2 Cognitive Interpretation

Such transitions may correspond to:

- sleep–wake cycles,

- anesthesia onset and emergence,

- attentional reset events,

- spread of global workspace activation.

Thus nonlinear RSVP dynamics supply a unified spectral account of physiological and cognitive phase transitions.

Appendix K: Computational Experiments for RSVP Spectra

This appendix presents computational techniques for validating the spectral predictions of RSVP through numerical discretizations.

K.1 Discrete RSVP Operator

Given a lattice with spacing h, approximate the Laplacian by

$$\nabla^2 \psi_i \approx \frac{1}{h^2} \sum_{j \in N(i)} (\psi_j - \psi_i).$$

The discretized linear RSVP operator is a block matrix

$$L_{\text{RSVP}}^{(h)} = \begin{pmatrix} A^{(h)} & B^{(h)} & C^{(h)} \\ D^{(h)} & E^{(h)} & F^{(h)} \\ G^{(h)} & H^{(h)} & J^{(h)} \end{pmatrix}.$$

K.2 Spectral Diagnostics

Compute:

1. eigenvalue spacings s_i,
2. unfolded spacing histograms,
3. two- and three-point correlation functions,
4. spectral rigidity $\Delta_3(L)$.

Compare these to GOE, GUE, Poisson, and empirical cortical spectra.

K.3 Predictions

RSVP predicts:

$$
\begin{aligned}
&\text{High-entropy: GOE/GUE universality,} \\
&\text{Low-entropy: coherent multi-band modes,} \\
&\text{Intermediate: zeta-like rigidity.}
\end{aligned}
$$

These provide concrete, falsifiable tests for the theory.

Appendix L: Index of Symbols and Glossary

This appendix summarizes the principal symbols, operators, fields, and mathematical objects appearing throughout the text. It is organized into four categories: spectral systems, RSVP field theory, operator structures, and neuroscientific constructs.

L.1 Spectral Systems

$\mathcal{H}_X$ Hilbert space associated with a system X (nucleus, zeta operator, cortex, RSVP).

$\mathcal{A}_X$ Operator algebra generated by the system operator: $\mathcal{A}_X = C^*(L_X)$.

L_X Primary linear operator governing dynamics or constraints for the system X.

μ_X Spectral measure induced by L_X on $\mathbb{R}$.

$R_k^{(X)}$ k-point correlation functions for the unfolded spectrum of L_X.

$\mathcal{E}(L)$ Spectrum (eigenvalues) of the operator L.

GOE, GUE

     Gaussian Orthogonal/Unitary Ensembles; universality classes for random spectra.

L.2 RSVP Fields and Plenum Dynamics

$\Phi(x,t)$ Scalar potential field of the RSVP plenum.

$v_\mu(x,t)$ Vector flow field (momentum-, drift-, or current-like component).

$S(x,t)$ Entropy density or entropic potential.

$g_{\mu\nu}$ Metric tensor on the plenum manifold M.

$\mathcal{S}$ Action functional for RSVP dynamics: $\mathcal{S} = \int \mathcal{L}\sqrt{|g|}\, dx\, dt$.

L_{RSVP} Linearized RSVP operator acting on perturbations ($\delta\Phi, \delta v, \delta S$).

$\mathcal{N}(\Phi, v, S)$ Nonlinear interaction functional governing higher-order coupling.

L.3 Differential and Operator Structures

∇, ∇_μ Covariant derivative induced by $g_{\mu\nu}$.

Δ_g Laplace–Beltrami operator on (M, g): $\Delta_g = \frac{1}{\sqrt{|g|}}\partial_i(\sqrt{|g|}g^{ij}\partial_j)$.

$F_{\mu\nu}$ Field-strength-like tensor associated with v_μ: $F_{\mu\nu} = \nabla_\mu v_\nu - \nabla_\nu v_\mu$.

A, B, C Coefficient matrices in the block form of L_{RSVP}.

U_ℓ Scaling operator implementing geometric dilation by factor ℓ.

$\beta(L_\ell)$ RG beta-function governing renormalization flow of operators.

L.4 Neuroscientific and Cognitive Constructs

L_{cortex} Effective cortical wave operator governing standing and traveling waves.

Cabral–Shemesh modes

     Macroscale standing-wave eigenmodes observed with ultrafast fMRI.

Traveling waves

     Propagating beta/gamma oscillations supporting working memory.

Rotating waves

     Cortical rotational modes controlling attentional resetting.

Mixed selectivity

     High-dimensional neural coding reduced to low-dimensional latent wave modes.

Spectral regime

     Global oscillatory structure (coherent, incoherent, anesthetic, etc.)

L.5 RSVP Spectral Phases

Poisson   Uncorrelated eigenvalues; low-coherence regime.

GOE/GUE

     Universal chaotic regime; high entropy or symmetry-reduced limit.

Coherent   Structured, low-dimensional resonant wave regime (cortex-like).

References

Berry, Michael V. (1986). "Riemann's Zeta Function: A Model for Quantum Chaos?" In: *Proceedings of the Royal Society A* 400, pp. 229–251.

Cabral, Joana, Francisca F. Fernandes, and Noam Shemesh (2023). "Intrinsic Macroscale Oscillatory Modes Driving Long-Range Functional Connectivity in Female Rat Brains Detected by Ultrafast fMRI". In: *Nature Communications* 14, p. 375. DOI: `10.1038/s41467-023-36072-6`.

Dyson, Freeman J. (1962). "Statistical Theory of the Energy Levels of Complex Systems". In: *Journal of Mathematical Physics* 3, pp. 140–156.

Firk, Frank W. K. and Steven J. Miller (2009). "Nuclei, Primes and the Random Matrix Connection". In: *Symmetry* 1.1, pp. 64–105. DOI: `10.3390/sym1010064`. arXiv: `0909.4914` [`math.NT`].

Han, H.-B. et al. (2024). "Rotating Brain Waves Help the Mind Refocus After Distraction". In: *MIT/Picower Report*.

Montgomery, Hugh L. (1973). "The Pair Correlation of Zeros of the Zeta Function". In: *Proc. Symposia in Pure Mathematics* 24, pp. 181–193.

Odlyzko, Andrew M. (1987). "On the Distribution of Spacings Between Zeros of the Zeta Function". In: *Mathematics of Computation* 48, pp. 273–308.

Trongnetrpunya, Apirak et al. (2022). "Traveling Waves in the Prefrontal Cortex During Working Memory". In: *Nature Communications* 13, p. 825. DOI: `10.1038/s41467-022-28451-9`.

Wigner, Eugene P. (1957). *Statistical Properties of Real Symmetric Matrices*. Academic Press.